Pythia 8.3 tuning based on Belle fragmentation related measurements

Ralf Seidl[1,2,3]

[1] *Tokyo University, QNSI, Tokyo, Japan*
[2] *RIKEN Nishina Center for Accelerator-Based Science, Wako, Saitama 351-0198, Japan*
[3] *RIKEN-BNL Research Center, Upton New York 11973-5000, USA*

January 13, 2026
v. 2.0

Abstract

Belle has measured a large number of fragmentation-related results that have been already successfully used in global fits of fragmentation functions. These fragmentation functions are important input for studying the nucleon structure in semi-inclusive Deeply inelastic lepton nucleon scattering and hadron collisions. Apart from the additional flavor-sensitivity, also spin and transverse momentum of partons in the nucleon can accessed this way. Additionally, these fragmentation-related results should be extremely sensitive to the fragmentation parameters in Monte Carlo event generators. This note concentrates on the tuning efforts of PYTHIA 8.3 using these measurements.

Contents

List of Figures

1 To-Do list and Changelog

1.1 README

1.2 To-Do list

- add sensitivity discussion for popcorn variables

1.3 Changelog v1.0 → v2.0

- Added candle plot with best values in comparison to default and Belle2 values

2 Introduction

Fragmentation describes the formation of confined final–state hadrons from high-energetic, asymptotically free partons. Just as parton distribution functions, they cannot be calculated from first principles in QCD and therefore need to be extracted experimentally. For the same reason, also Monte Carlo event generators have to use models to describe this. One of the most commonly used models is the Lund string fragmentation model. While the Lund model can describe the fragmentation reasonably well, overall, it relies on many parameters that need to be tuned using data. In this note this tuning was performed systematically on the various fragmentation measurements that contain sensitivities to the main Lund parameters, the suppression of strange quark pairs produced in the fragmentation, the suppression of η mesons, the suppression of di-quark pair production needed to create baryons in the fragmentation, the transverse momentum generated in the fragmentation, and the role vector mesons and higher spin particle production has over the pseudoscalar production, etc.

In the following the procedure to tune the fragmentation parameters are discussed. Initially the different types of software and their setups are discussed. Then, the sensitivities of the used measurements to the relevant variables are discussed before the actual fit results and best tune parameters are presented and discussed.

2.1 The Lund Model

The Lund String fragmentation model [1, 2] is the main model that tries to describe the fragmentation process. It generally describes e^+e^- fragmentation into hadrons as the separation of singlet (anti)quarks moving away from each other within a linear potential that quasi-classically describes the QCD confining potential. The linear potential can be thought of being caused by a string of gluons connecting the two color charges. This string then eventually breaks up into a quark-antiquark pair (or also diquark-antidiquark pair). These resulting (anti-)quarks either coalesce into hadrons or expand further, creating even more quark-antiquark pairs in the process. In this stochastic process particles are then produced according to

$$f(z) = N\frac{1}{z}(1-z)^a \exp\left(-\frac{bm^2}{z}\right) \tag{1}$$

where a defines how fast the function vanishes at high-z and b is related to the mass created at a certain z, and z is the energy fraction a hadron carries relative to the initial parton energy. Furthermore, this generation does not have to necessarily follow on the lightcone, but can also happen at transverse coordinates, thus allowing for transverse momentum to be generated relative to the initially separating partons. Empirically, not all quark-antiquark pairs can be created equally, as heavier quarks are less likely to be created in the fragmentation process. For this purpose a parameter was introduced that describes the suppression of strangeness relative to light quark flavors. The model is initially also not a priori able to distinguish between what spin-state a certain hadron that was created has. Therefore parameters for vector meson generation over pseudo-scalar generation for light, strange and

charm quarks are introduced, as well as similar parameters for spin, orbital angular and total angular momenta up to 2 are introduced.

3 Tuning Setup, prerequisites, etc

For the general setup, Pythia 8.3.12 (later also 8.3.16 to be discussed below, see A) was used where the main144 code of the examples section was utilized to enable the facility to parse input files and provide yoda output files that are using the RIVET analysis codes for the data sets specified below. RIVET4.0.1 was was used for the analysis codes, Rivet plotting and the actual data yoda files. A few significant exceptions to this are that the most recent Belle measurements for light and charmed mesons [3] were not available yet, therefore yoda data files, Rivet analysis codes and plotting instructions were created personally to include them in the tuning. Similarly, a few issues were found in the official RIVET codes that were fixed locally. Those include a switching of the ordering of integrated hyperon and charmed baryon cross sections relative to those differential in the momentum fraction. Also for the transverse momentum dependent measurements, the fractional energy z binning in the codes was off by one bin for protons that would be physically impossible to cover at Belle energies due to its mass. Also for some measurements the treatment of weak decays was inaccurate as only charmed decays were removed in the RIVET codes while other weak decays were kept, in contrast to the actual measurements. Therefore the weak-decay removed measurements that include pions or protons were not included in the fitting procedure. The tune optimization was performed using the Professor2.5 package [4].

4 Data sets used in the fitting

For the fitting, the following measurements were used, ordered by publication time:

4.1 BELLE_2017_I1606201

These measurements include various hyperon and charmed baryon final states as a function of the fractional momentum x_p and the total production cross sections [5]. Because of these, these measurements are particularly sensitive to the Baryon production related PYTHIA variables.

4.2 BELLE_2017_I1607562

These measurements contain the invariant mass and fractional energy dependent cross sections for same and opposite charged pairs of pions and kaons within the same hemisphere [6]. As such, they provide information on the various mass peaks in their range and therefore also indirectly on higher spin and orbital momentum particles that feed into these spectra.

4.3 BELLE_2019_I1718551

These measurements contain the cross sections of pions, kaons and protons as a function of energy fraction z and transverse momentum relative to the thrust axis, in bins of the thrust value [7]. Therefore they are most sensitive to the transverse momentum generation in the fragmentation, but indirectly also the main LUND related fragmentation variables, etc.

4.4 BELLE_2020_I1777678

In this publication the cross sections as a function of fractional energy z for pions, kaons and protons are included, being likely sensitive to the main Lund fragmentation parameters, as well as the baryon related ones for the protons [8]. Additionally, also pairs of pions or kaons in same or opposite hemispheres as well as any pairs are measured as function of the fractional energies of each hadron. Apart from the nominal fractional energy definition two alternate definitions are also included, however for this exercise they were not included in the tuning effort since those would be mostly redundant.

4.5 BELLE_2024_I2849895

This is the newest result, just published earlier in 2025, and contains a larger number of cross sections differential in the momentum fraction x_p for various lighter and charmed mesons decaying into two or three pions or kaons, many for the first time at B factories [3]. This data set is most sensitive to the pseudo-scalar to vector-meson ratios, the η suppression, the light pseudo-scalar and vector mixing angles, and indirectly also the higher spin resonances.

5 Sample generation, etc

Given that the number of datasets that are used are very large, it was not possible to fit all tuning parameters at the same time. Instead, parameter sets of 6 to 8 were optimized simultaneously while iterating over all relevant parameters and preforming the optimization many times to avoid running into local minima. In each iteration the best values of the previous tune were set while the next set of variables were allowed to float. In the initial iterations the parameter ranges were mostly identical to the allowed ranges in PYTHIA while in the later iterations, the ranges were narrowed down somewhat for variables that were very stable over the previous steps. In PROFESSOR, the initial configurations are randomly created based on the boundaries of the variables to optimize using the command *prof2-sample*. In earlier iterations about 500 to 1000 samples were generated while in the later stages 2000 samples were generated. This ensured that the interpolation of the parameter tunes and responses could be performed using 5th order polynomials, still. For each sample initially 1.2 M and later 5 M $e^+e^- \to q\bar{q}$ events were generated for uds and charm flavors together. As all these measurements had already been corrected for non-$q\bar{q}$

Table 1: Parameters used in the tuning, their PYTHIA8.3 default values, the BelleII default values (as of release-09-00-01 in generators/modules/fragmentation/-data/pythia_belle2_charm.dat), empty if PYTHIA 8.2 default value is used, the best value after the tuning and a brief explanation of the parameter.

Variable	P8.3	Belle2	Best	description
StringZ:aLund	**0.68**	**0.32**	**0.525**	**(1-z) power**
StringZ:bLund	0.98	0.62	0.910	Transverse mass term
StringPT:sigma	0.335		0.372	Transverse momentum in fragmentation
StringFlav:probStoUD	0.217	0.286	0.240	Strangeness suppression wrt to ud quarks
StringFlav:etaSup	0.60		0.850	Extra eta suppression
StringFragmentation:stopMass	1.0	0.3	0.831	Stop mass (End point condition?)
StringFlav:mesonUDVector	0.50		0.554	Vector to PS ratio light quarks
StringFlav:mesonUDL1S0J1	0.0		0.311	Higher spin states L=1, S=0, J=1 light q
StringFlav:mesonUDL1S1J0	0.0		0.236	Higher spin states L=1, S=1, J=0 light q
StringFlav:mesonUDL1S1J1	0.0		0.267	Higher spin states L=1, S=1, J=1 light quarks
StringFlav:mesonUDL1S1J2	0.0		0.400	Higher spin states L=1, S=1, J=2 light quarks
StringFlav:mesonSvector	0.55		0.870	Vector to PS ratio strange quarks
StringFlav:mesonSDL1S0J1	0.0		0.118	Higher spin states L=1, S=0, J=1 s quarks
StringFlav:mesonSDL1S1J0	0.0		0.374	Higher spin states L=1, S=1, J=0 s quarks
StringFlav:mesonSDL1S1J1	0.0		0.365	Higher spin states L=1, S=1, J=1/2 s quarks
StringFlav:mesonSDL1S1J2	0.0		0.588	Higher spin states L=1, S=1, J=1/2 s quarks
StringZ:rFactC	1.32	1.0	0.410	Bowler modification for charm quarks
StringFlav:mesonCvector	0.88	2.8	2.226	Vector to PS ratio charm quarks
StringFlav:mesonCDL1S0J1	0.0	0.06	1.729	Higher spin states L=1, S=0, J=1 charm
StringFlav:mesonCDL1S1J0	0.0	0.1775	0.635	Higher spin states L=1, S=1, J=0 charm
StringFlav:mesonCDL1S1J1	0.0	0.1868	2.644	Higher spin states L=1, S=1, J=1 charm
StringFlav:mesonCDL1S1J2	0.0	0.1836	1.972	Higher spin states L=1, S=1, J=2 charm
StringFlav:thetaPS	-15		-15.71	Mixing angle for PS mesons
StringFlav:thetaV	36		27.08	Mixing angle for V mesons
StringFlav:probQQtoQ	0.081	0.133	0.064	Diquark over quark ratio
StringZ:aExtraDiquark	0.97		1.696	Lund extra a term for diquarks(baryons)
StringFlav:probSQtoQQ	0.9156	0.323	0.521	Strange over light diquark suppression
StringFlav:probQQ1toQQ0	0.0275	0.0468	0.252	Vector over scalar diquark suppression
StringFlav:popcornRate			0.055112	mesons between diquark pairs
StringFlav:popcornSpair			0.106073	strange Popcorn diquark
StringFlav:popcornSmeson			0.447140	strange meson in Popcorn

contributions, no other hard processes are included. Also ISR had been corrected in the measurements so it was switched off in the MC generation as well.

The following sets of parameters were optimized together initially:

- Set A (main Lund): StringZ:aLund, StringZ:bLund, StringPT:sigma, StringFlav:probStoUD, StringFlav:etaSup, StringFragmentation:stopMass
- Set B (baryons and charm): StringFlav:probQQtoQ, StringFlav:probSQtoQQ, StringFlav:probQQ1toQQ0, StringZ:aExtraDiquark, StringZ:rFactC, StringFlav:mesonCvector StringFlav:mesonCL1S0J1, StringFlav:mesonCL1S1J0
- Set C (vector mesons, mixing): StringFlav:mesonUDvector, StringFlav:mesonUDL1S0J1, StringFlav:mesonUDL1S1J0, StringFlav:mesonSvector, StringFlav:mesonSL1S0J1, StringFlav:mesonSL1S1J0,StringFlav:thetaPS,StringFlav:thetaV
- Set D (higher spin states): StringFlav:mesonUDL1S1J1, StringFlav:mesonUDL1S1J2, StringFlav:mesonSL1S1J1, StringFlav:mesonSL1S1J2, StringFlav:mesonCL1S1J1,

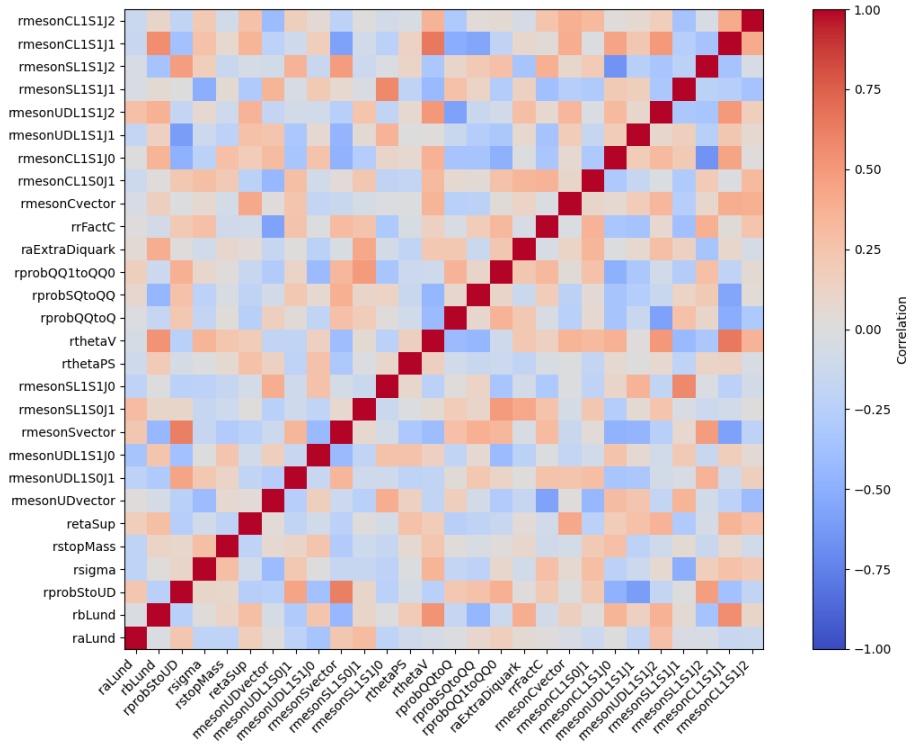

Figure 1: Correlation matrix of all parameters as obtained from a test tuning set that was run over 5000 parameters, a reduced set of data sets and only a third order interpolation in order to be computationally feasible at all.

StringFlav:mesonCL1S1J2

As can be seen in Fig. 1, all these 28 parameters are not uncorrelated, nor do the parameters of each set factorize either but generally they are somewhat less correlated between sets. Because of this an iterative approach was used where sets A to D were optimized several times after optimizing each set first (i.e. A→B→C→D→A→B→etc.) The individual correlation matrices after the last iteration of each tuning set are shown in Fig. 2. As one can see, within a tuning set correlations are more pronounced, most notably between the main two Lund parameters, but also, to a lesser extend between others.

At later iterations of the optimization, the more stable variables were retired (StringPT:sigma, StringFlav:probStoUD, StringFlav:mesonUDvector, StringFlav:probQQtoQ), using their best values from then on, but including the additional higher spin states and eventually the popcorn variables. The later settings therefore became:

- Set A' (main Lund): StringZ:aLund, StringZ:bLund, StringFlav:etaSup, StringFragmentation:stopMass, mesonUDL1S0J1, mesonUDL1S1J0
- Set B' (baryons): StringFlav:probSQtoQQ, StringFlav:probQQ1toQQ0, StringZ:aExtraDiquark popcornRate, StringFlav:popcornSpair, StringFlav:popcornSmeson
- Set C' (strange+mixing): StringFlav:mesonSvector, StringFlav:mesonSL1S0J1,

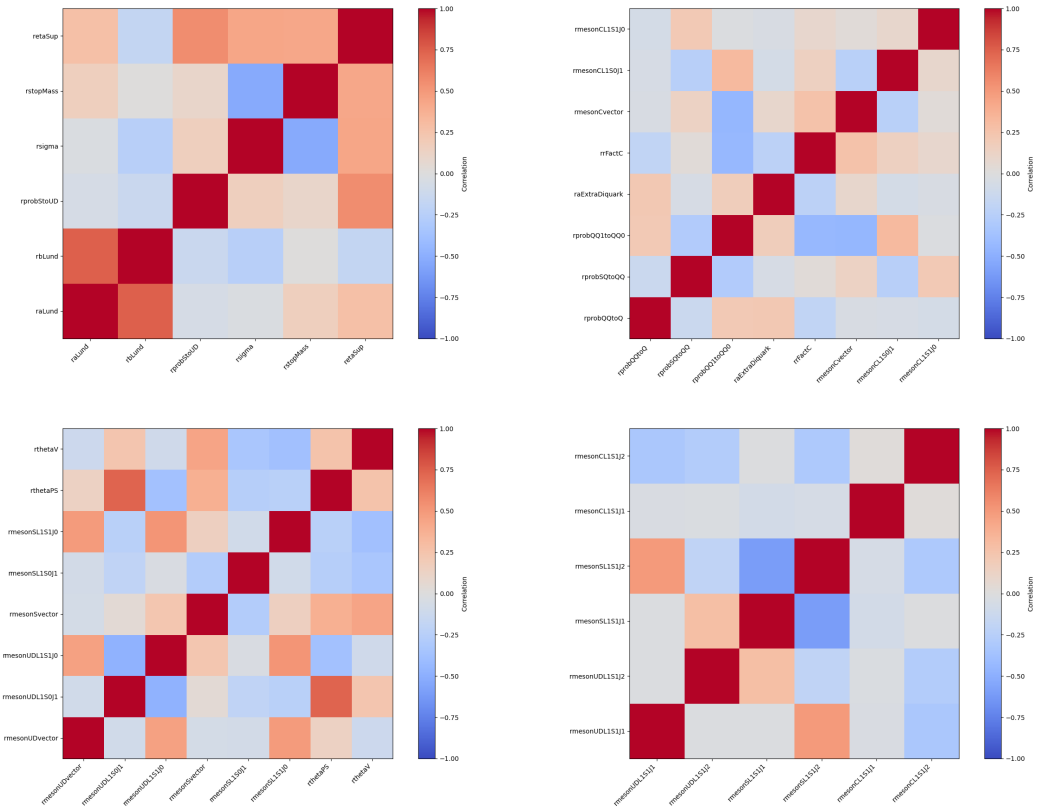

Figure 2: Correlation matrices of each tuning set separately, obtained from the last iterations of the nominal tuning procedure and interpolation based on 2000 parameter sets each, the full data sets and a 5th order polynomial interpolation.

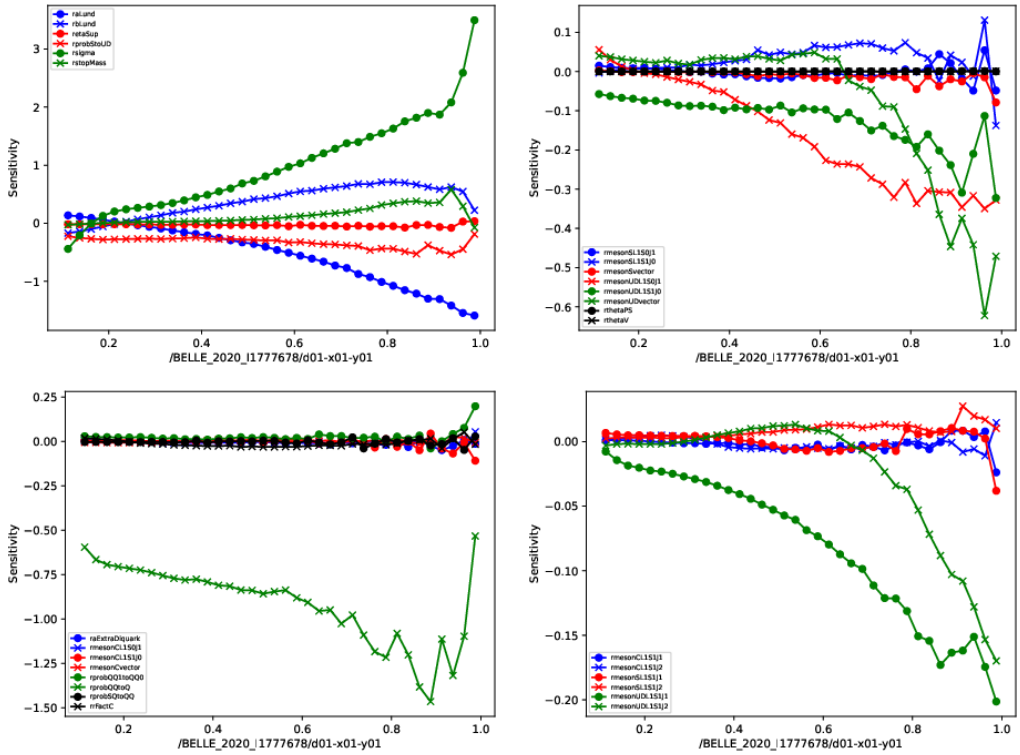

Figure 3: Sensitivities of the pion cross sections as a function of the fractional energy z. The diffenent curves correspond to the sensitivities to the various tune parameters.

StringFlav:mesonSL1S1J0, StringFlav:mesonSL1S1J1, StringFlav:mesonSL1S1J2, StringFlav:thetaPS, StringFlav:thetaV

- Set D' (charm): StringZ:rFactC, StringFlav:mesonCvector, StringFlav:mesonCL1S0J1, StringFlav:mesonCL1S1J 0, StringFlav:mesonCL1S1J1, StringFlav:mesonCL1S1J2

6 Individual sensitivities

In the following the individual sensitivities to the various tune parameters are shown for several of the key measurements.

6.1 Single hadron cross sections

This single pion cross sections have naturally a very high sensitivity to the main Lund fragmentation parameters, as well as to the fragmentation transverse momentum as can be seen in Fig. 3. There is also some sensitivity to the light quark vector mesons to pseudoscalar ratios and higher spin states. For kaons the sensitivities are similar except that strangeness suppression and the corresponding strange quark VM and higher spin variables are more sensitive as can be seen in Fig. 4. Protons in contrast are mostly sensitive to the diquark ratio and to a lesser extend the main Lund parameters.

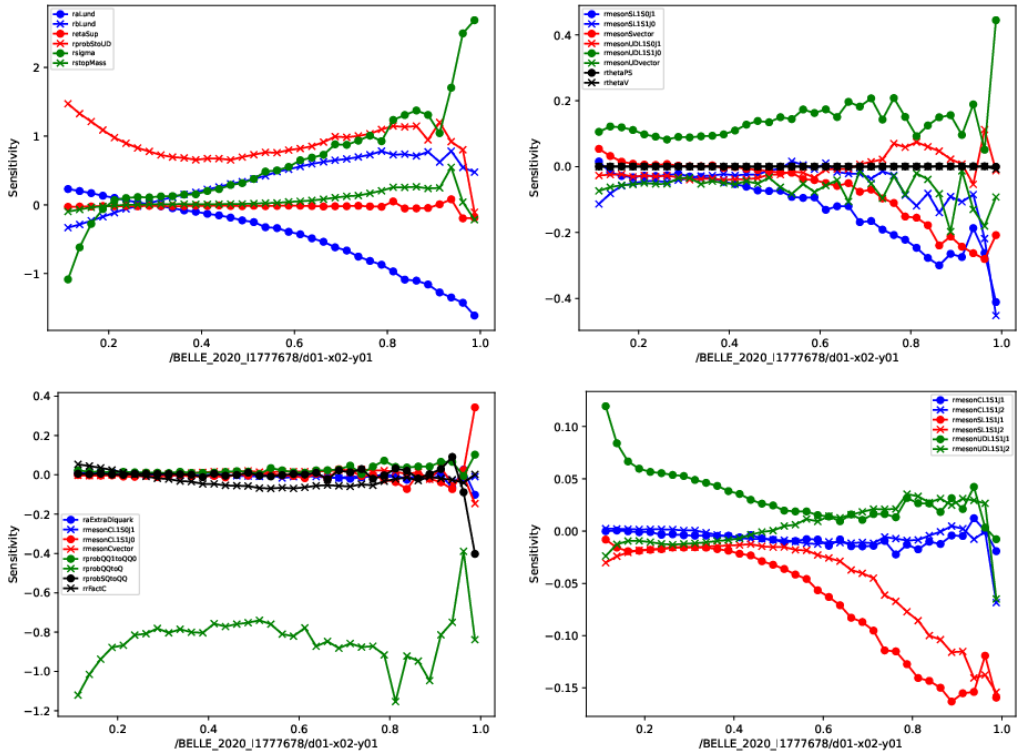

Figure 4: Sensitivities of the kaon cross sections as a function of the fractional energy z. The different curves correspond to the sensitivities to the various tune parameters.

For the vector mesons cross sections, the vector mesons variables for the relevant flavors are clearly the most sensitive parameters as can be seen in Fig. 6 for the ρ mesons, Fig. 7 for the ω Fig. 8, for the K^* and Fig. 9 for the ϕ mesons. The strange mesons do also have some sensitivity to the strangeness suppression again.

The η mesons naturally are most sensitive to the eta suppression parameter while they also provide a small sensitivity to the pseudoscalar mixing angle, apart from the regular Lund parameters, as shown in Fig. 10.

The charmed mesons obtain additional sensitivity to the extra charm term for the fragmentation, as well as for the vector mesons to the charmed VM hand higher spin state variables.

6.2 Di-hadron cross sections

For the di-hadron cross sections, again the vector mesons components appear in the vicinity of their masses, while additionally some sensitivity to the higher spin mesons is visible, particularly at higher masses as those can mostly be only indirectly obtained in these di-hadron spectra.

6.3 Transverse momentum dependent cross sections

The transverse momentum dependent cross sections naturally have a very high sensitivity to the transverse momentum generated in the fragmentation process as can

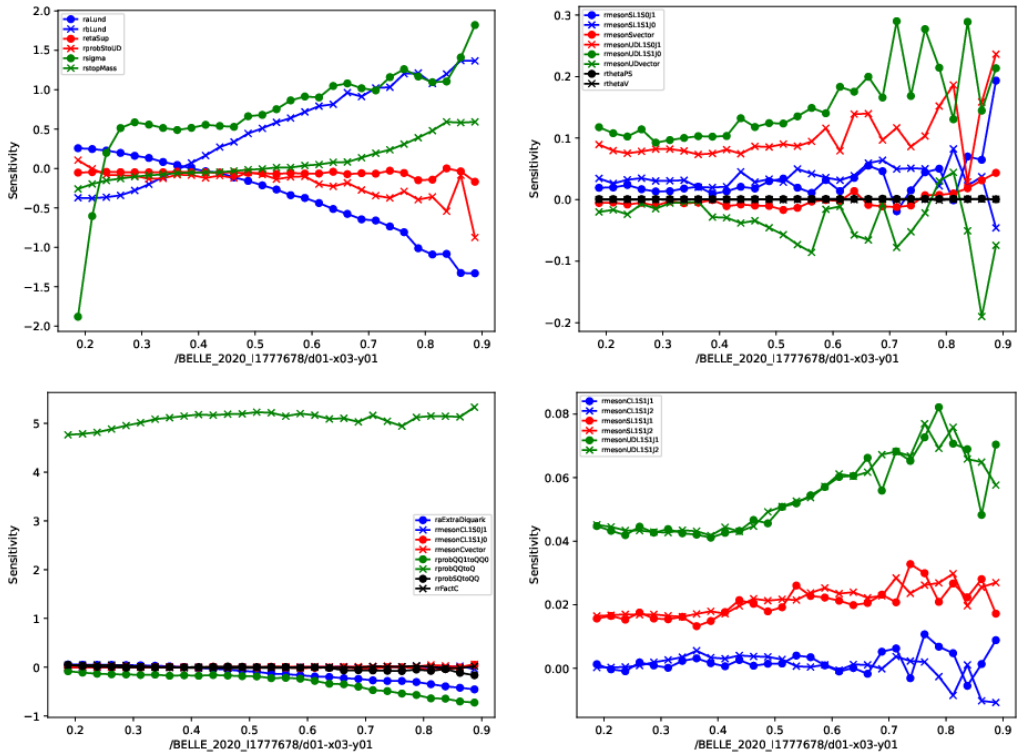

Figure 5: Sensitivities of the proton cross sections as a function of the fractional energy z. The different curves correspond to the sensitivities to the various tune parameters.

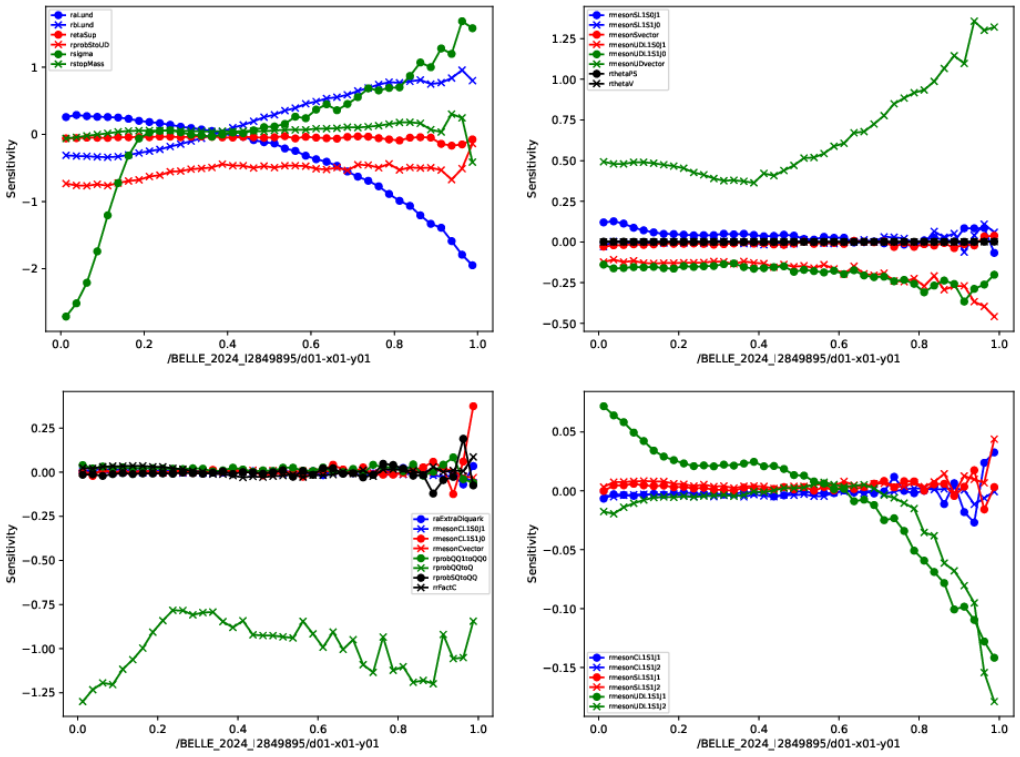

Figure 6: Sensitivities of the ρ^0 cross sections as a function of the fractional energy x_p. The different curves correspond to the sensitivities to the various tune parameters.

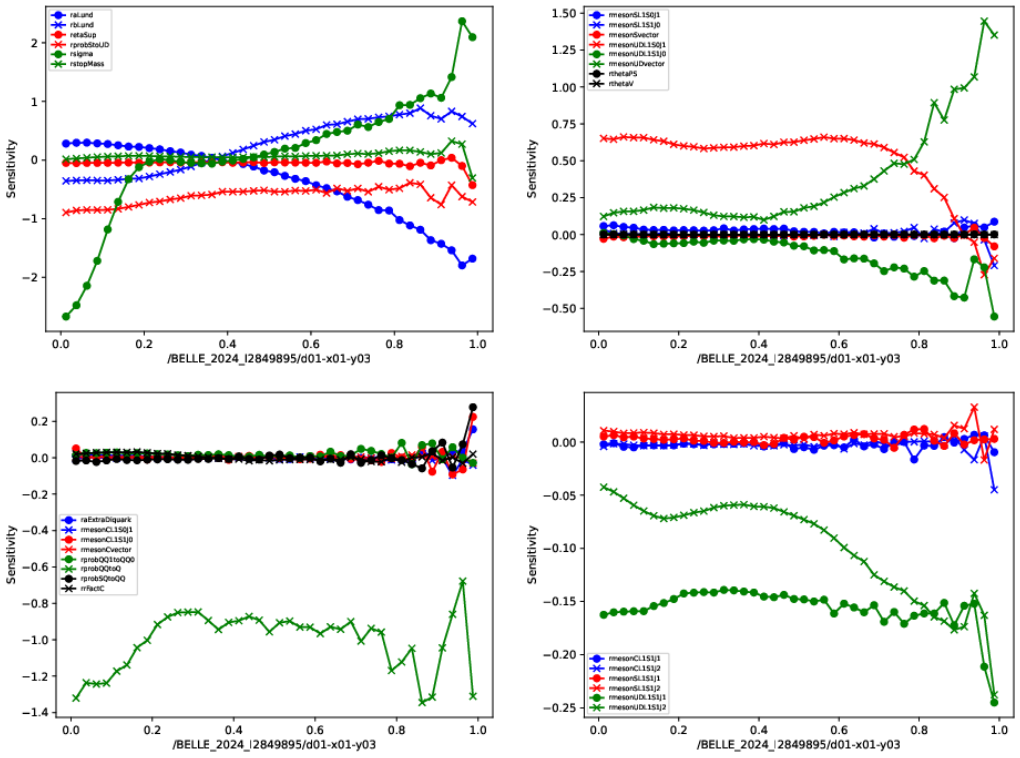

Figure 7: Sensitivities of the ω cross sections as a function of the fractional energy x_p. The different curves correspond to the sensitivities to the various tune parameters.

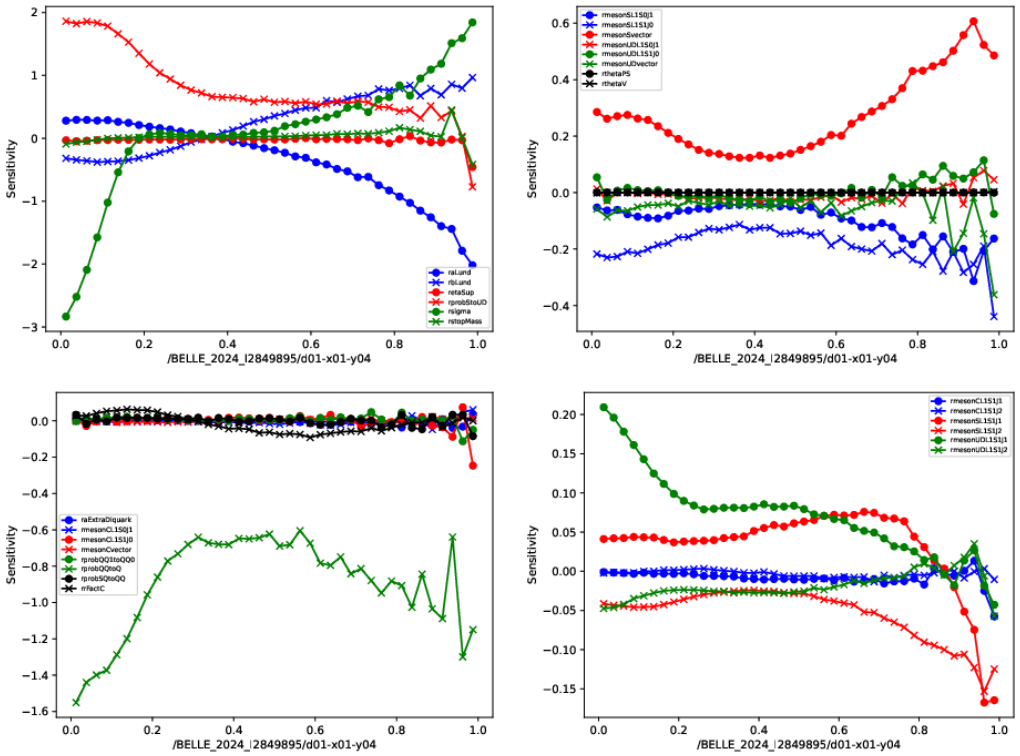

Figure 8: Sensitivities of the K^{*0} cross sections as a function of the fractional energy x_p. The different curves correspond to the sensitivities to the various tune parameters.

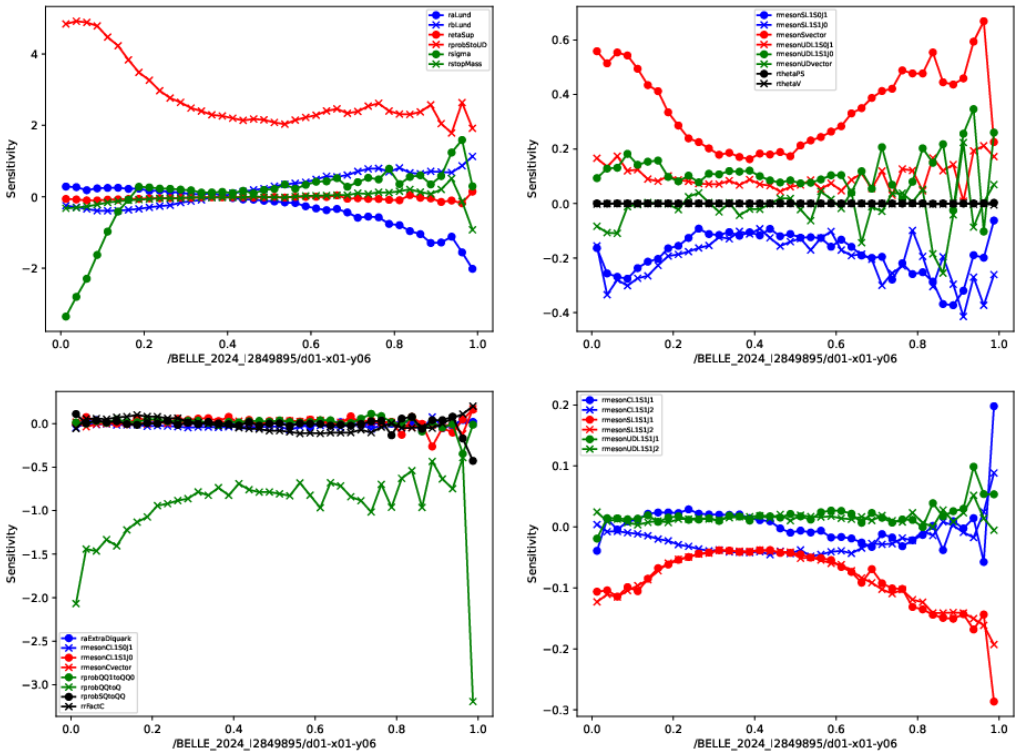

Figure 9: Sensitivities of the ϕ cross sections as a function of the fractional energy x_p. The different curves correspond to the sensitivities to the various tune parameters.

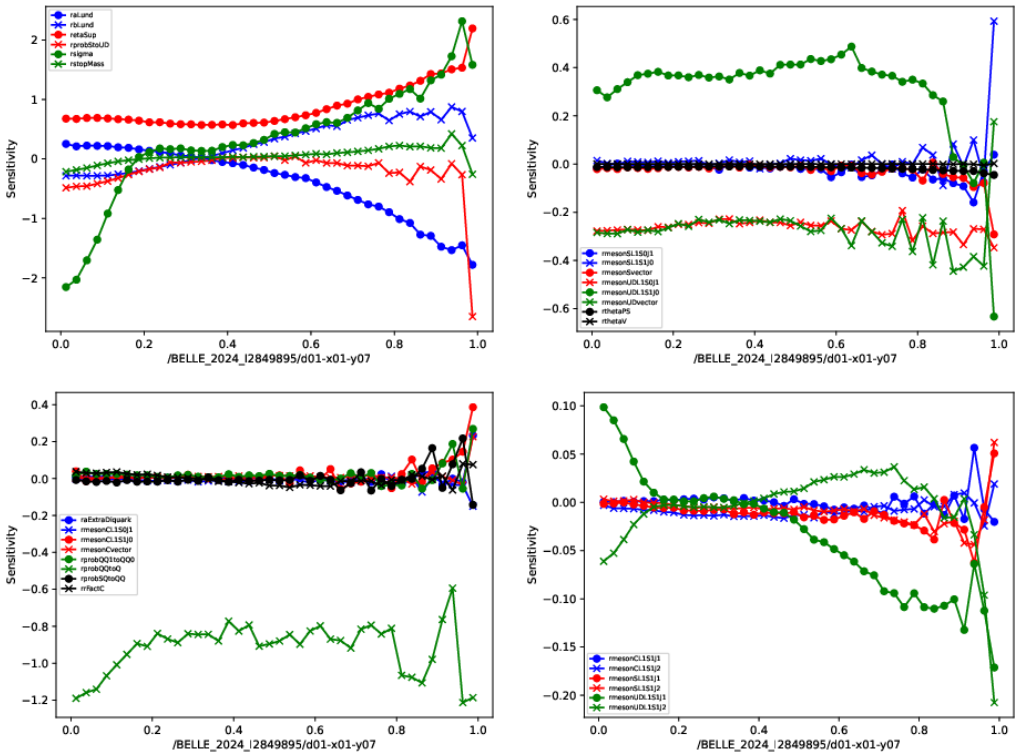

Figure 10: Sensitivities of the η cross sections as a function of the fractional energy x_p. The different curves correspond to the sensitivities to the various tune parameters.

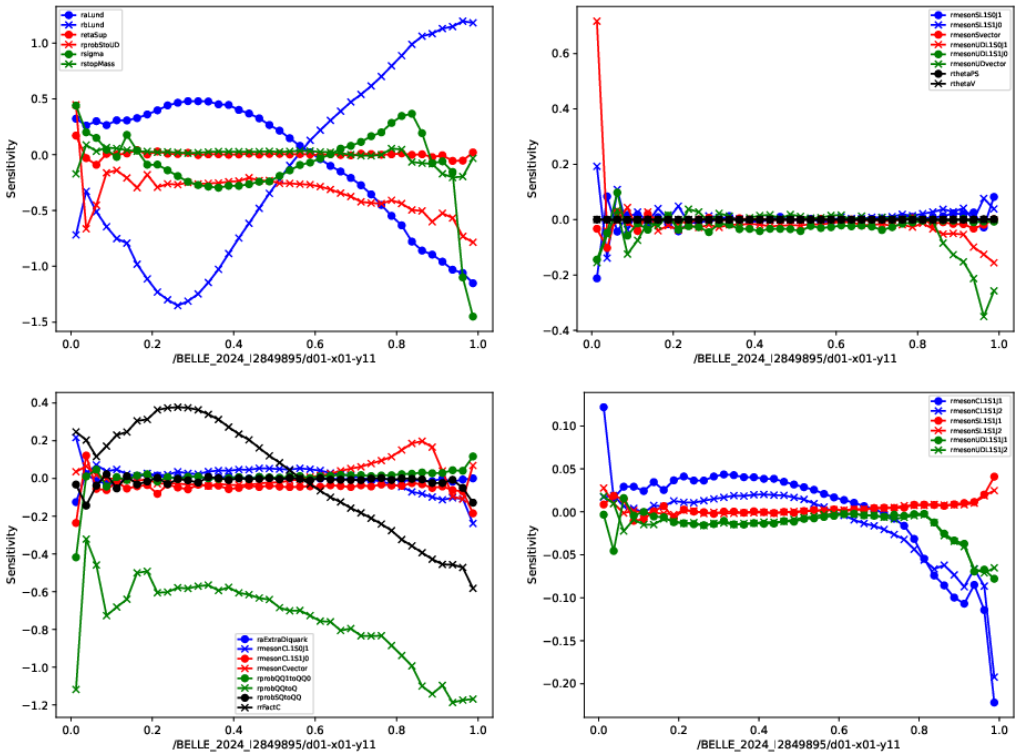

Figure 11: Sensitivities of the D^+ cross sections as a function of the fractional energy x_p. The different curves correspond to the sensitivities to the various tune parameters.

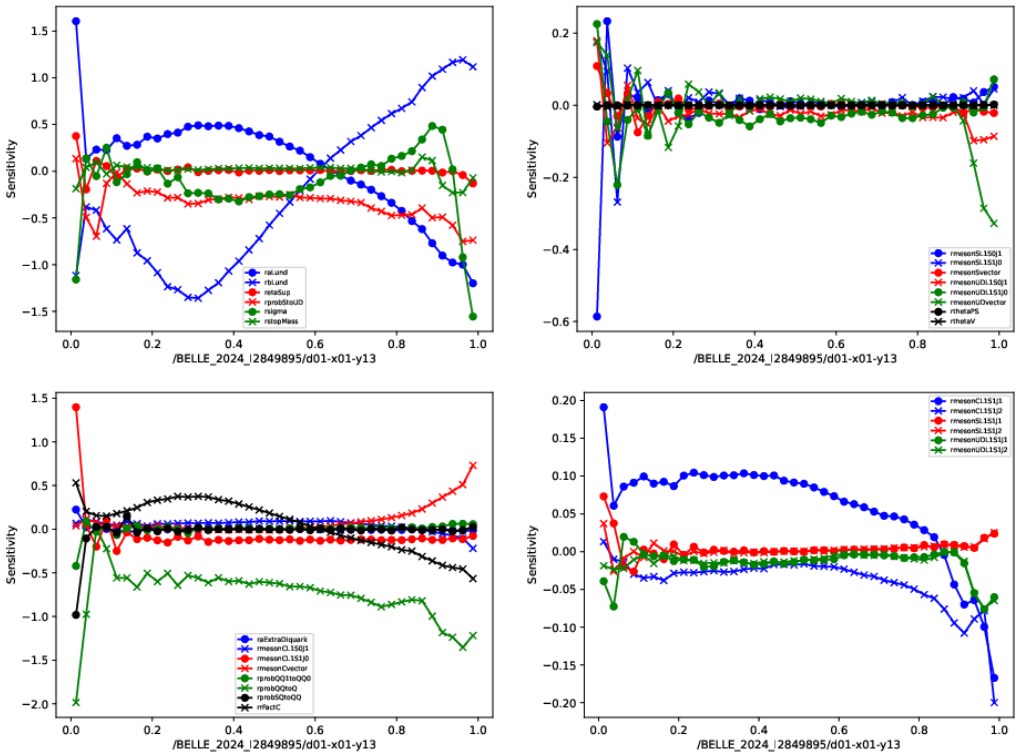

Figure 12: Sensitivities of the D^{*0} cross sections as a function of the fractional energy x_p. The different curves correspond to the sensitivities to the various tune parameters.

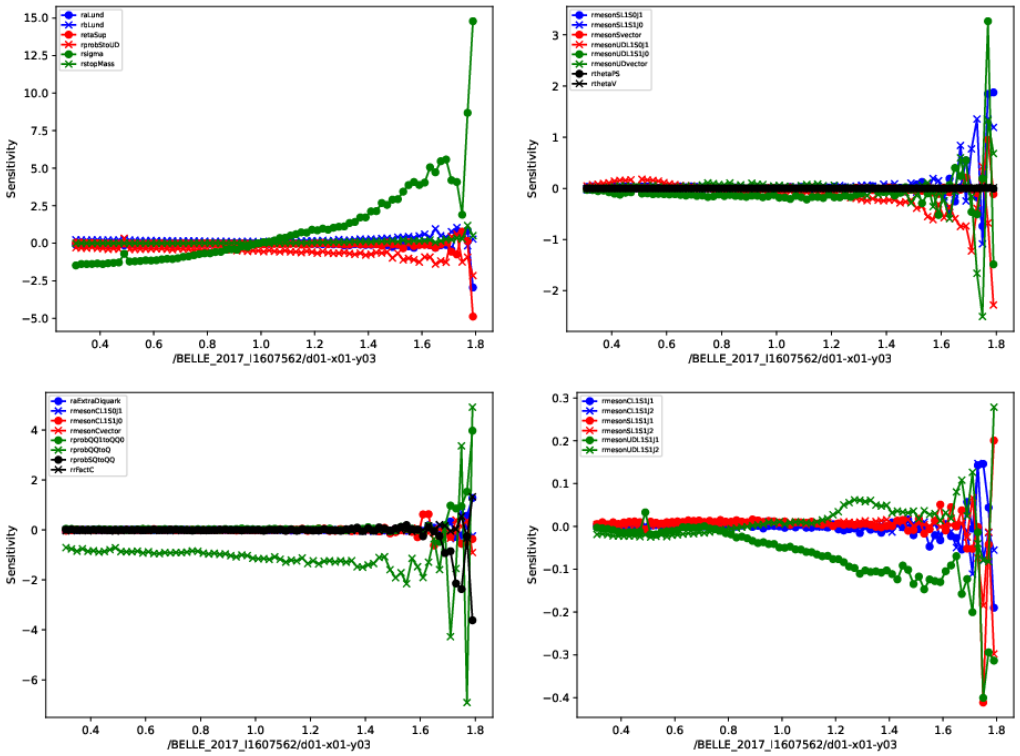

Figure 13: Sensitivities of the $\pi^+\pi^-$ cross sections as a function of the invariant mass, in the z bin . The different curves correspond to the sensitivities to the various tune parameters.

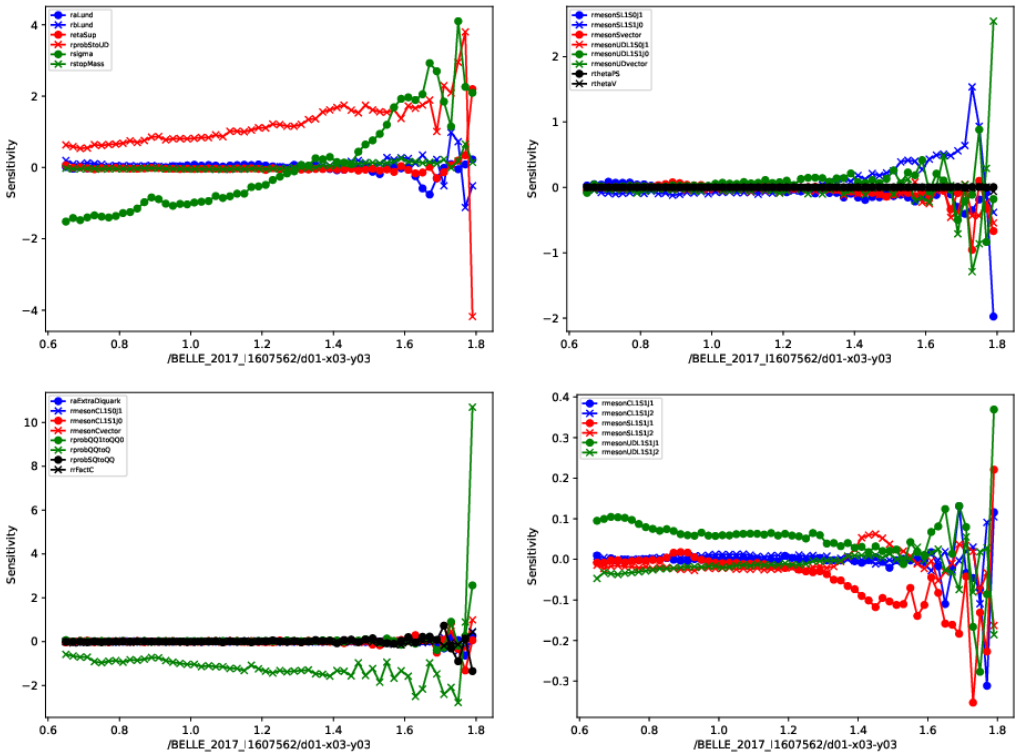

Figure 14: Sensitivities of the π^+K^- cross sections as a function of the invariant mass, in the z bin . The different curves correspond to the sensitivities to the various tune parameters.

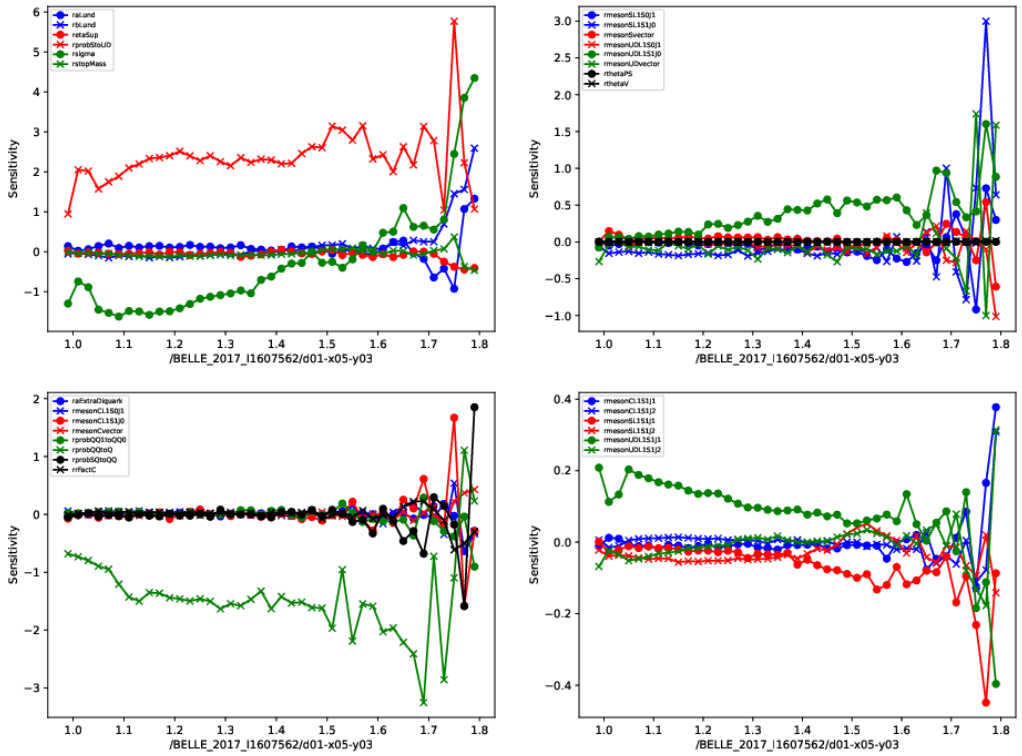

Figure 15: Sensitivities of the K^+K^- cross sections as a function of the invariant mass, in the z bin. The different curves correspond to the sensitivities to the various tune parameters.

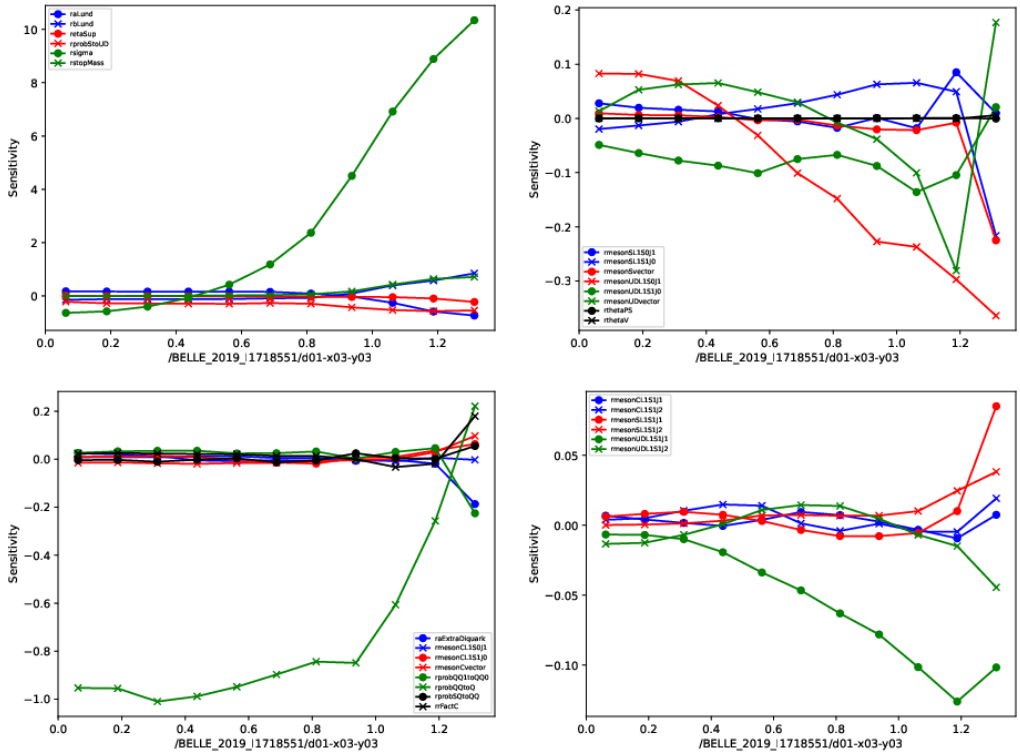

Figure 16: Sensitivities of the π cross sections as a function of the transverse momentum in the z bin and a thrust value of $0.8-0.9$. The different curves correspond to the sensitivities to the various tune parameters.

be seen in Figs. 16 to 18.

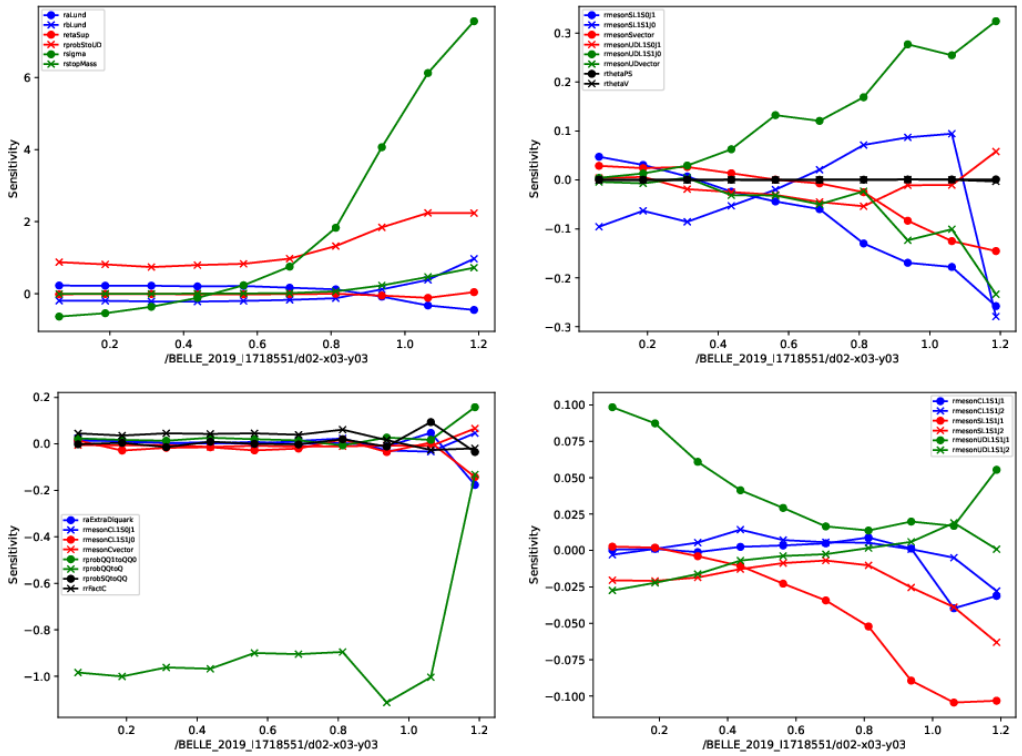

Figure 17: Sensitivities of the π cross sections as a function of the transverse momentum in the z bin and a thrust value of $0.8-0.9$. The different curves correspond to the sensitivities to the various tune parameters.

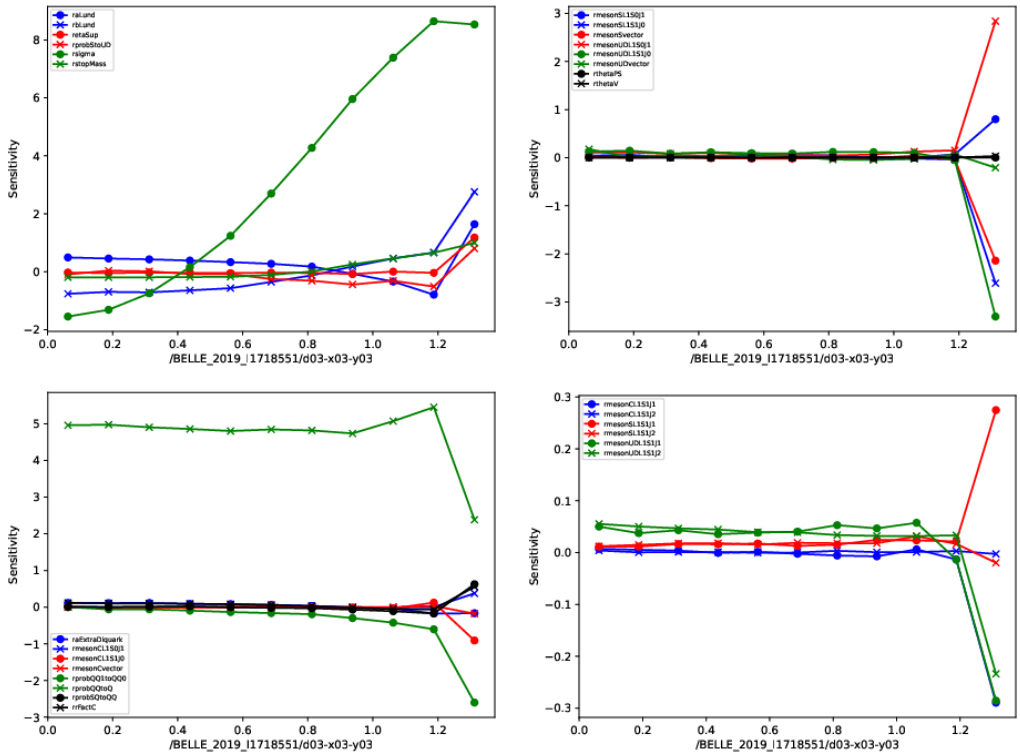

Figure 18: Sensitivities of the π cross sections as a function of the transverse momentum in the z bin and a thrust value of $0.8 - 0.9$. The different curves correspond to the sensitivities to the various tune parameters.

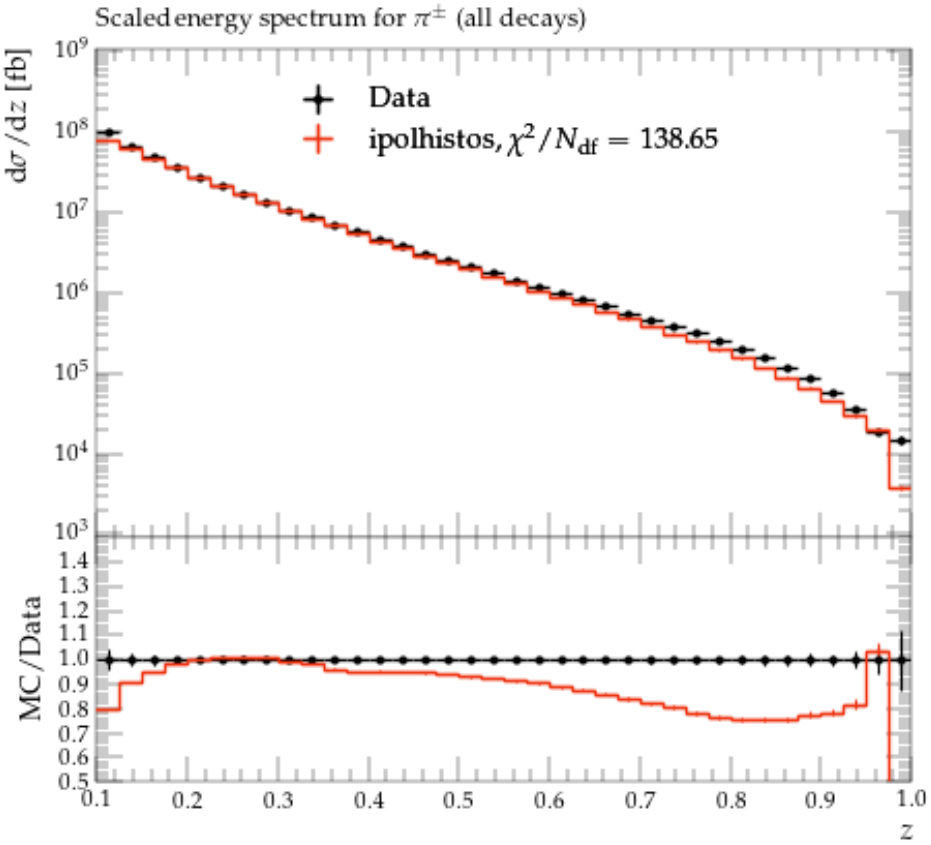

Figure 19: Pion cross sections as a function of the fractional energy z. The data is displayed by black points while the best fit result in red.

7 Tuning fits

7.1 Main hadrons

The best results can be seen in Fig. 19 to 21 for the main pion, kaon and proton cross sections. One can see that for the mesons the data can be described reasonably well overall, while the high precision of the pion data still results in fairly high χ^2. The proton data cannot be described so well which appears to be a common problem for baryon production in the Lund model as will be apparent from the other baryon related results below.

7.2 Decaying and charmed mesons

For the various light mesons that were studied in publication [3], the tuning efforts are able to provide a good description of the data and generally low χ^2. Those fit results are displayed in Figs. 22 to 25.

Charmed mesons are also mostly well described, with the vector mesons comparing particularly well, as can be seen in Figs. 26 to 28. On the strange D mesons are slightly less well described as apparently the additional shift in the peak positions due to the heavier strange quarks cannot be well accommodated in the Lund model.

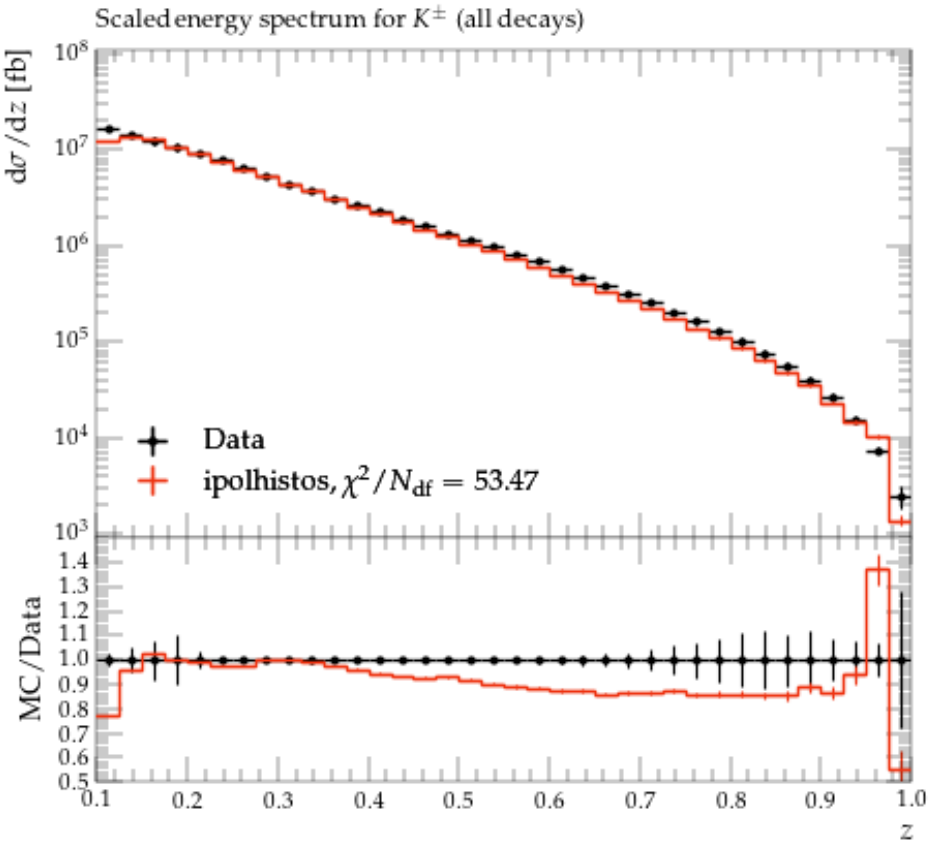

Figure 20: Kaon cross sections as a function of the fractional energy z. The data is displayed by black points while the best fit result in red.

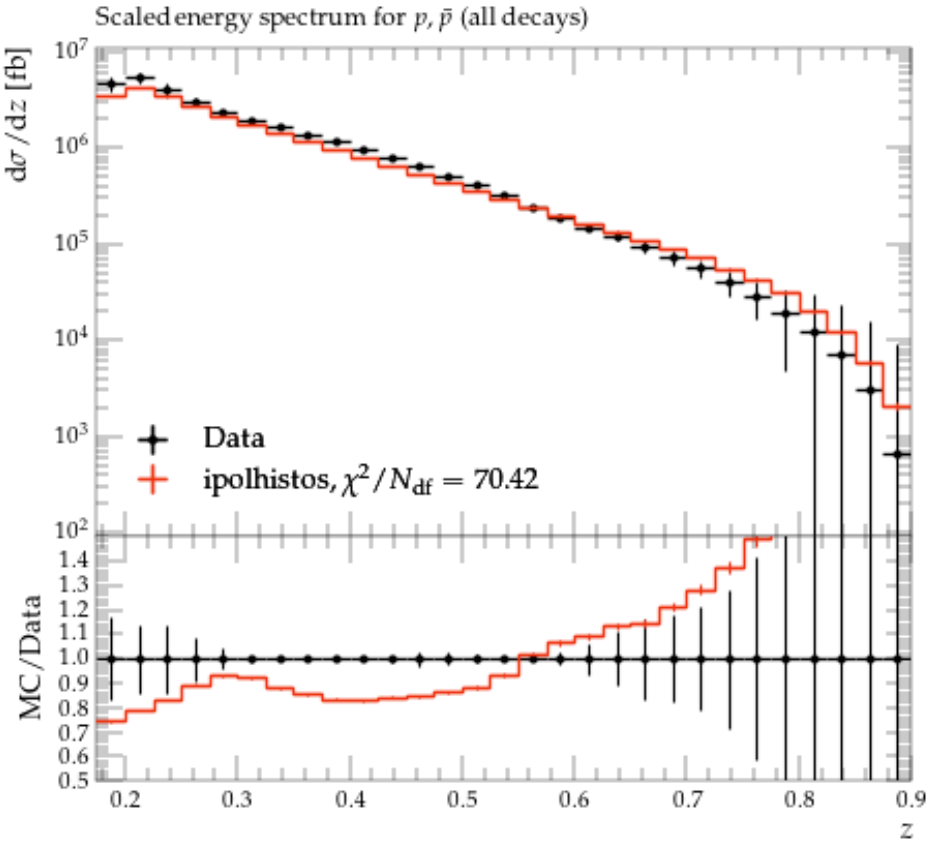

Figure 21: Proton cross sections as a function of the fractional energy z. The data is displayed by black points while the best fit result in red.

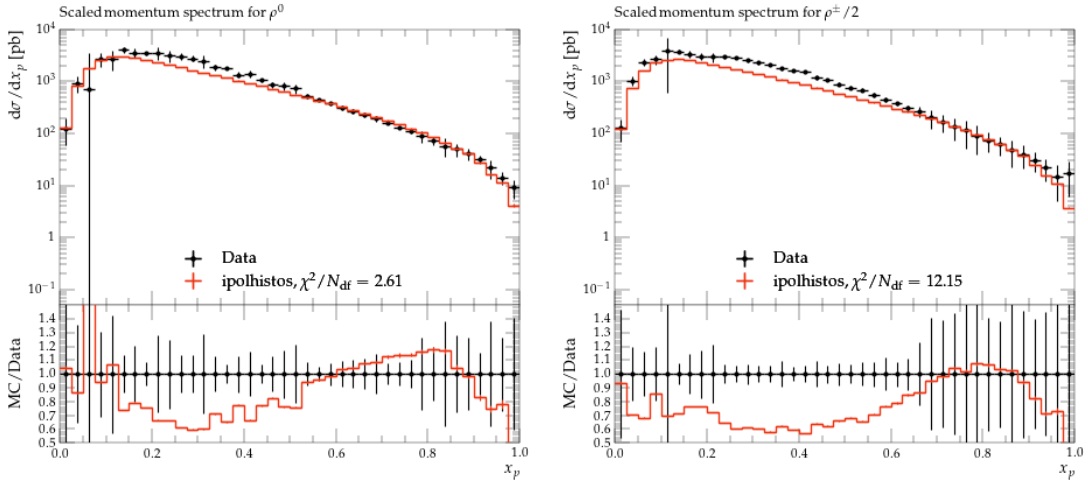

Figure 22: Left: neutral ρ cross sections as a function of the fractional momentum x_p. Right: charged ρ cross sections. The data is displayed by black points while the best fit result in red.

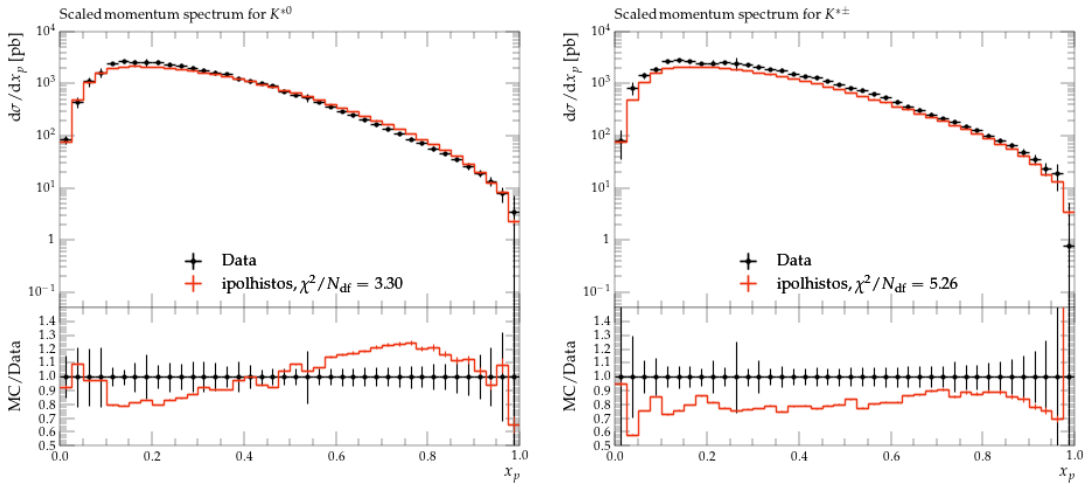

Figure 23: Left: neutral K^* cross sections as a function of the fractional momentum x_p. Right: charged K^* cross sections. The data is displayed by black points while the best fit result in red.

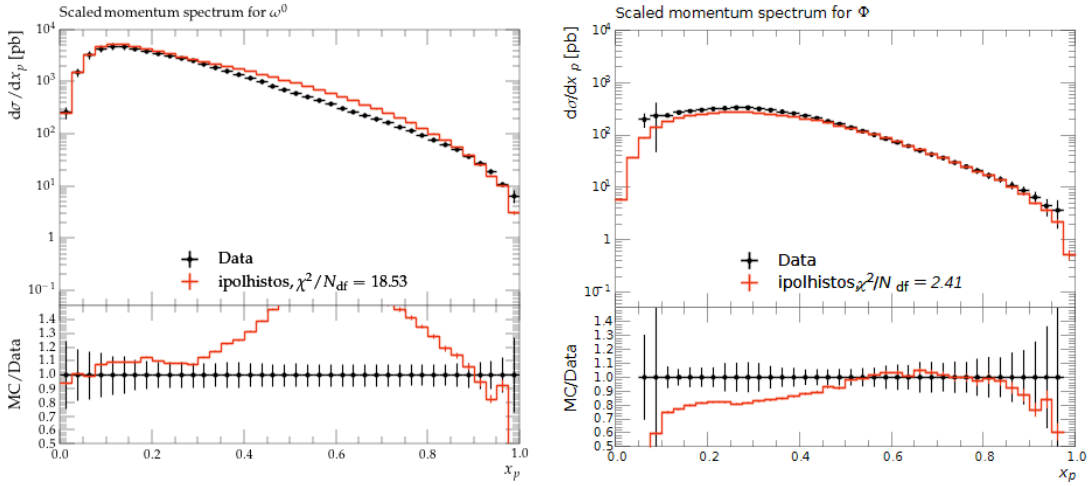

Figure 24: Left: ω cross sections as a function of the fractional momentum x_p. Right: ϕ cross sections. The data is displayed by black points while the best fit result in red. The missing χ^2 is 3.96.

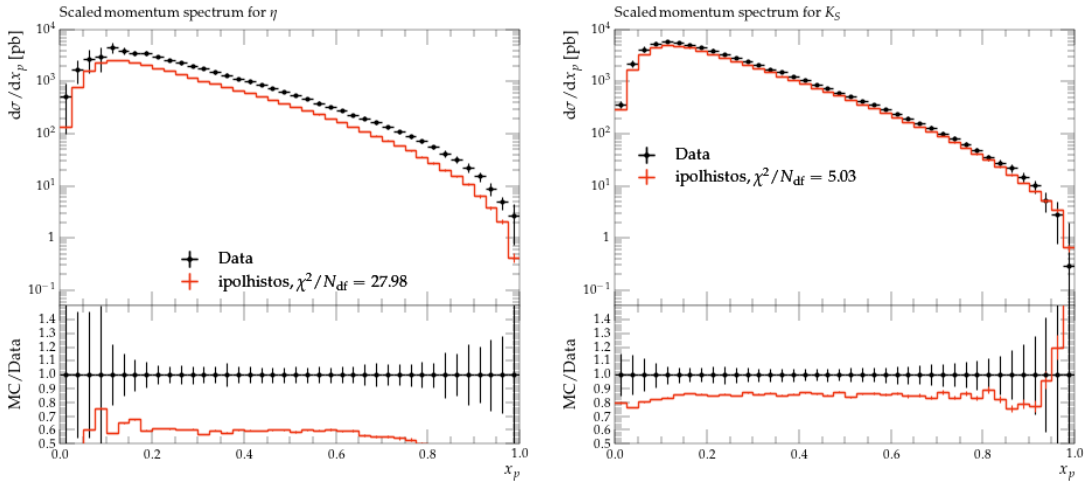

Figure 25: Left: η cross sections as a function of the fractional momentum x_p. Right: K_S cross sections. The data is displayed by black points while the best fit result in red.

In the figures the χ^2 values are often given as nans, since Rivet cannot deal with empty bins, but they were added by hand based on the professor tuning outcome which does provide them correctly.

7.3 Di-hadrons in various configurations

In the following, examples of the dihadron invariant mass distributions are shown for one low and one higher fractional energy bin in Figs. 29 to 34. One can see that for many hadron combinations, the overall description is good, but some features are not well reproduced. Most notably in the opposite-sign pion-kaon spectra the bump at around 1.5 GeV is not as pronounced in the MC, or rather somewhat elongated in comparison to the data, As the underlying decay of D mesons into $K\pi\pi$ is also present in PYTHIA, likely some of the details are not as well described there compared to EvtGen (as the bump was very clearly visible in the Belle I MC as well). Another aspect that is not well described are the same-sign pion pair's low mass region which generally underestimates the amount of pairs. For pion-kaon and kaon pairs the description is generally quite resonable also at lower masses.

Also the back-to-back di-hadron distributions as a function of fractional energies, the description of the data by the best tune is again very reasonable, as shown in Figs. 35 to 40 for selected fractional energy bin and hadron type combinations.

7.4 Transverse momentum dependent cross sections

The transverse momentum dependent cross sections are also fairly well described, particularly the low transverse momentum region that most directly is sensitive to the transverse momentum generated in the fragmentation process. In the higher transverse momentum tails, some slight differences can be seen, albeit with rather large uncertainties on the measurements.

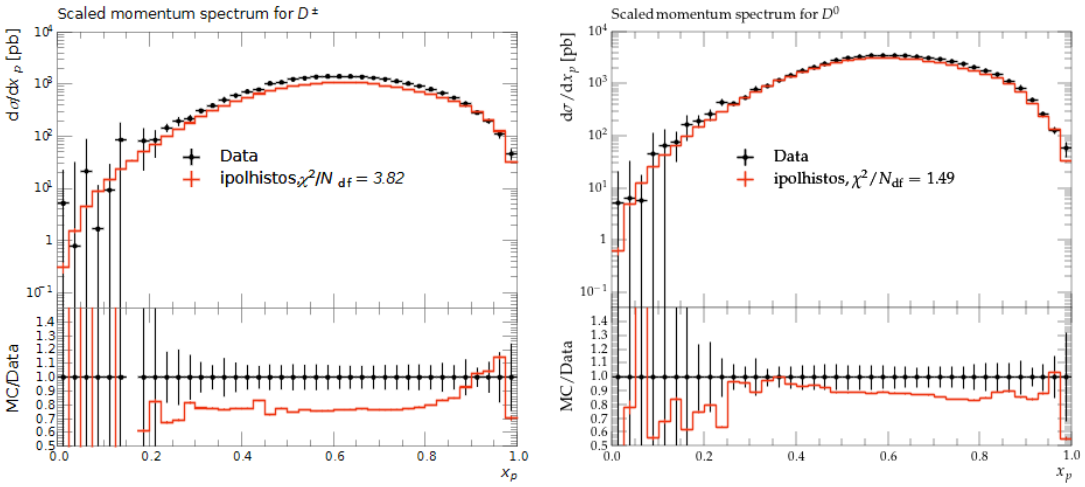

Figure 26: Left: D^+ cross sections as a function of the fractional momentum x_p. Right: D^0 cross sections. The data is displayed by black points while the best fit result in red.

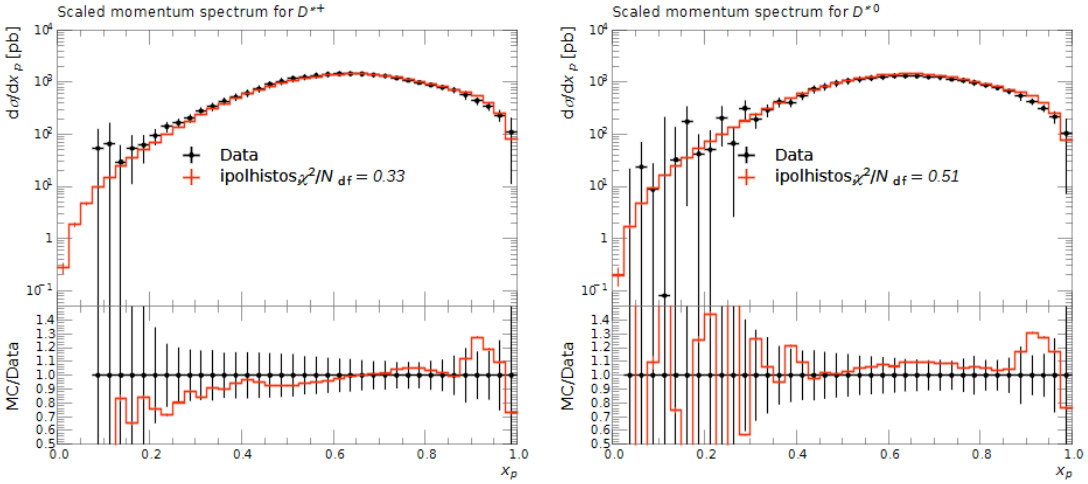

Figure 27: Left: D^{*+} cross sections as a function of the fractional momentum x_p. Right: D^{*0} cross sections. The data is displayed by black points while the best fit result in red.

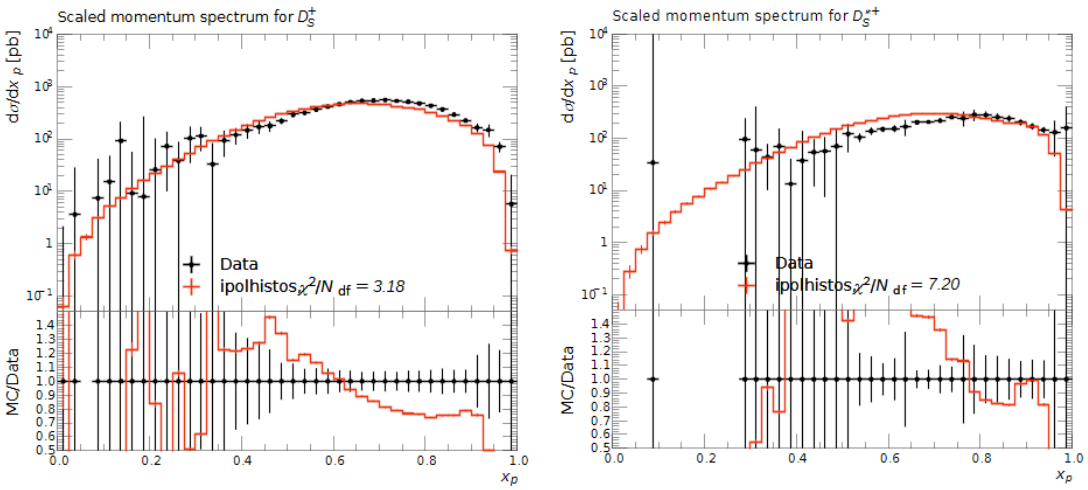

Figure 28: Left: D_s^+ cross sections as a function of the fractional momentum x_p. Right: D_s^{*+} cross sections. The data is displayed by black points while the best fit result in red.

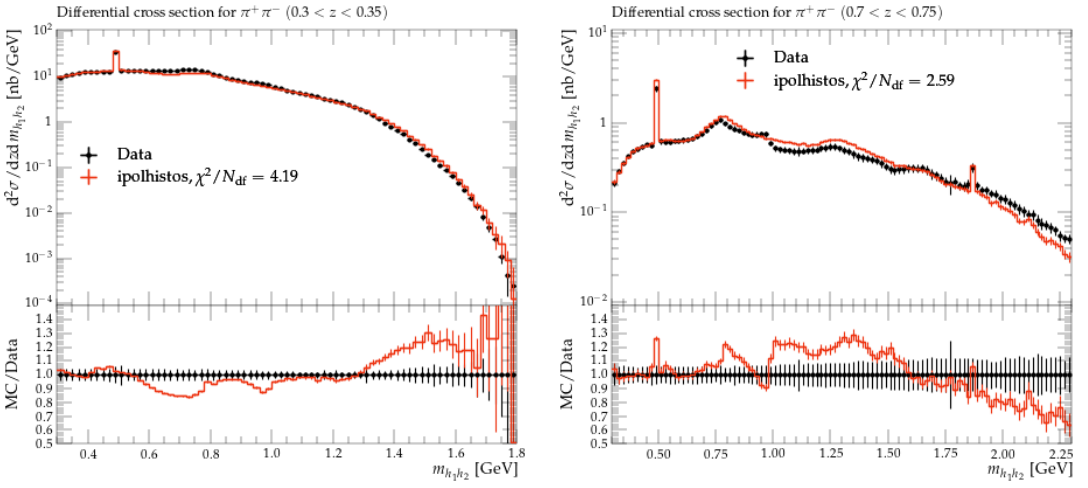

Figure 29: Left: $\pi^+\pi^-$ pair cross sections as a function of the invariant mass m for the fractional energy bin $0.3 - 0.35$. Right: The same for the fractional energy bin $0.7 - 0.75$. The data is displayed by black points while the best fit result in red.

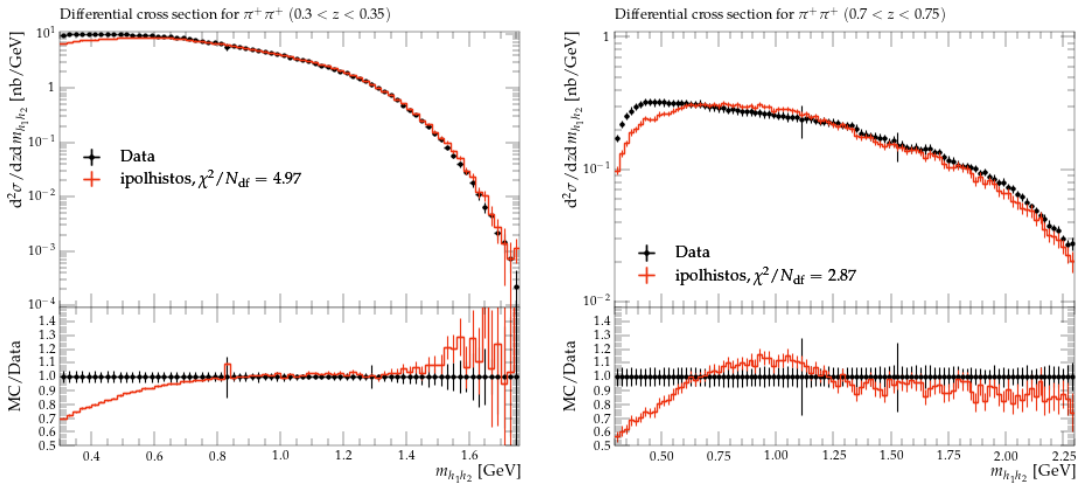

Figure 30: Left: $\pi^+\pi^+$ pair cross sections as a function of the invariant mass m for the fractional energy bin $0.3 - 0.35$. Right: The same for the fractional energy bin $0.7 - 0.75$. The data is displayed by black points while the best fit result in red.

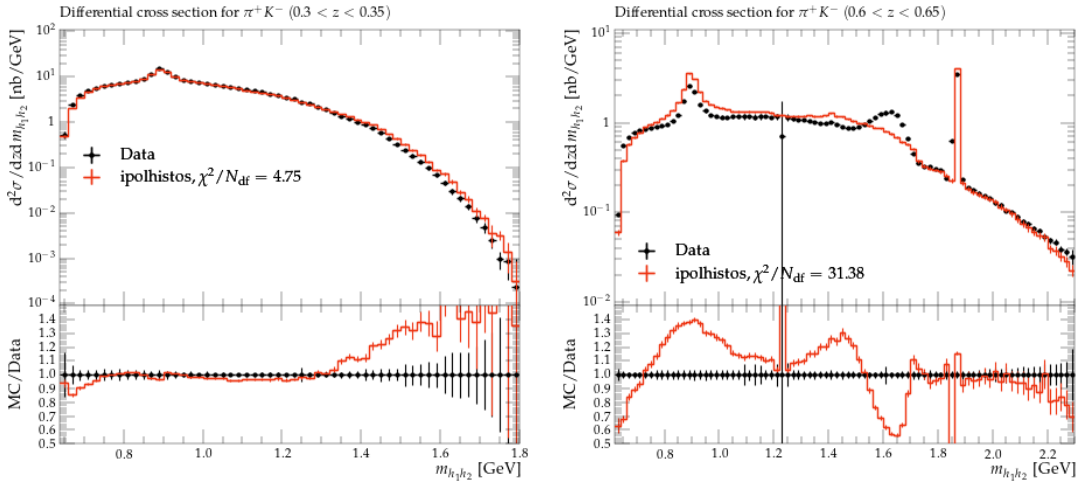

Figure 31: Left: π^+K^- pair cross sections as a function of the invariant mass m for the fractional energy bin $0.3 - 0.35$. Right: The same for the fractional energy bin $0.6 - 0.65$. The data is displayed by black points while the best fit result in red.

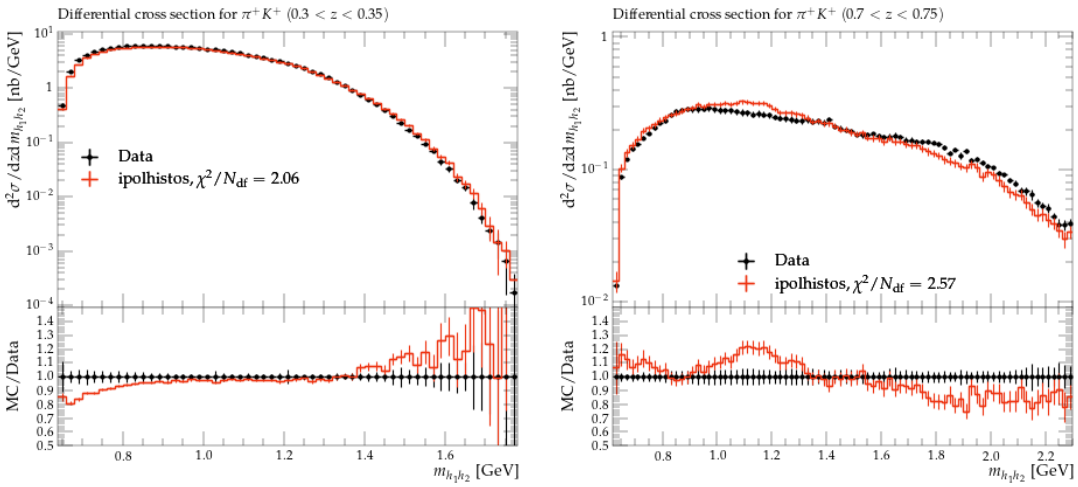

Figure 32: Left: π^+K^+ pair cross sections as a function of the invariant mass m for the fractional energy bin $0.3 - 0.35$. Right: The same for the fractional energy bin $0.7 - 0.75$. The data is displayed by black points while the best fit result in red.

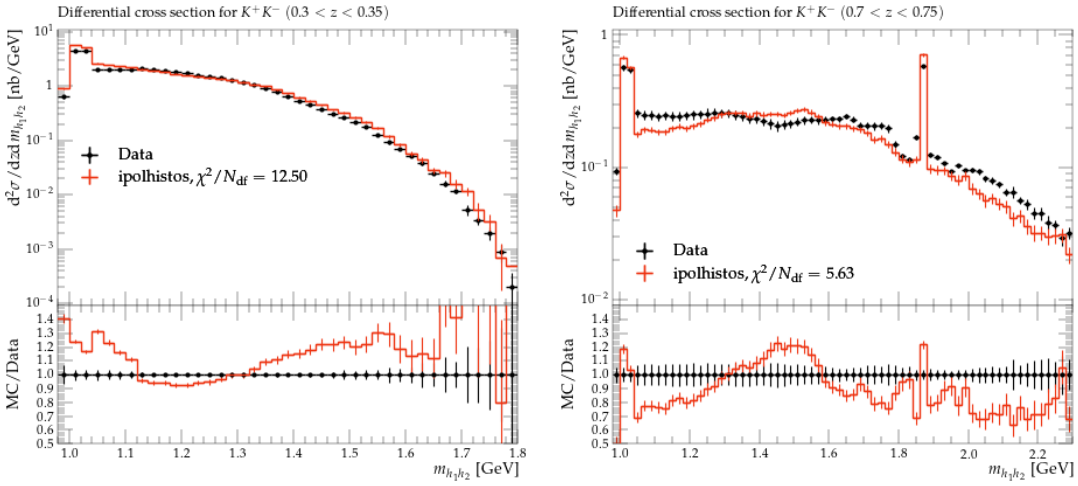

Figure 33: Left: K^+K^- pair cross sections as a function of the invariant mass m for the fractional energy bin $0.3 - 0.35$. Right: The same for the fractional energy bin $0.7 - 0.75$. The data is displayed by black points while the best fit result in red.

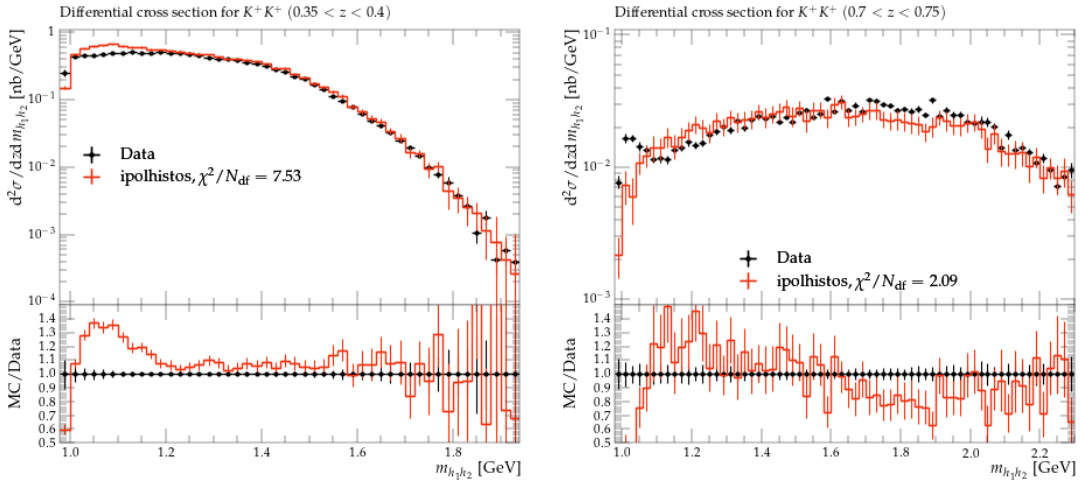

Figure 34: Left: K^+K^+ pair cross sections as a function of the invariant mass m for the fractional energy bin $0.35 - 0.4$. Right: The same for the fractional energy bin $0.7 - 0.75$. The data is displayed by black points while the best fit result in red.

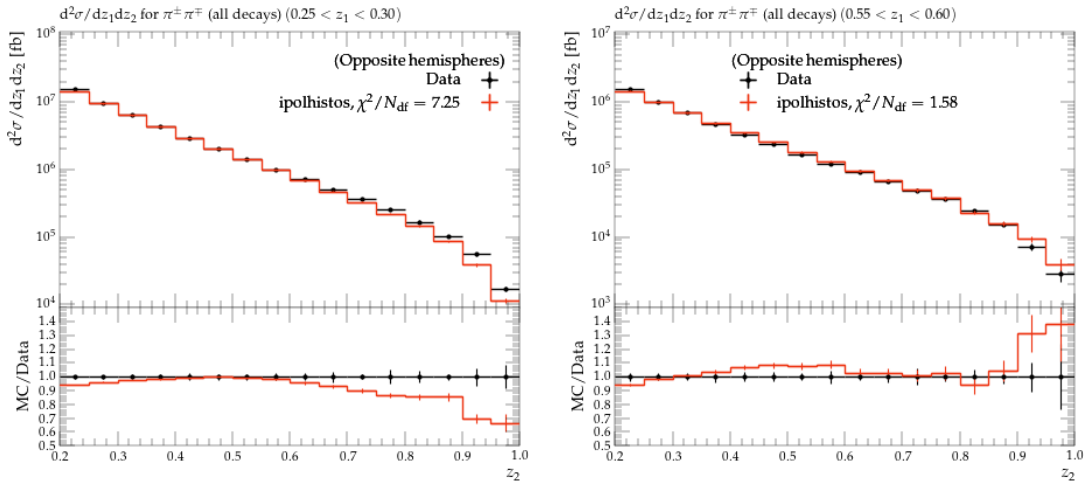

Figure 35: Left: $\pi^+\pi^-$ pair cross sections in opposite hemispheres as a function of the invariant mass z_2 for the fractional energy bin $0.25 < z_1 < 0.3$. Right: The same for the fractional energy bin $0.55 < z_1 < 0.6$. The data is displayed by black points while the best fit result in red.

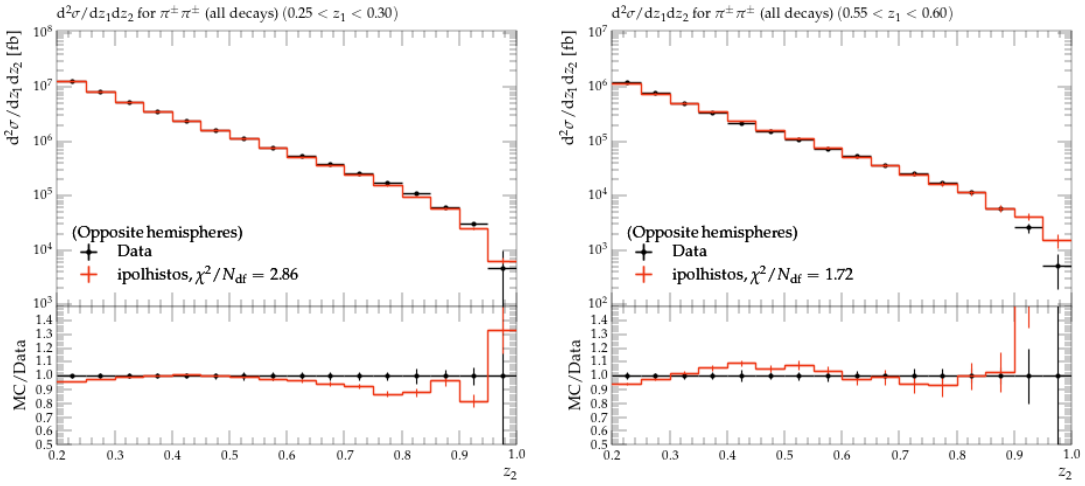

Figure 36: Left: $\pi^+\pi^+$ pair cross sections in opposite hemispheres as a function of the invariant mass z_2 for the fractional energy bin $0.25 < z_1 < 0.3$. Right: The same for the fractional energy bin $0.55 < z_1 < 0.6$. The data is displayed by black points while the best fit result in red.

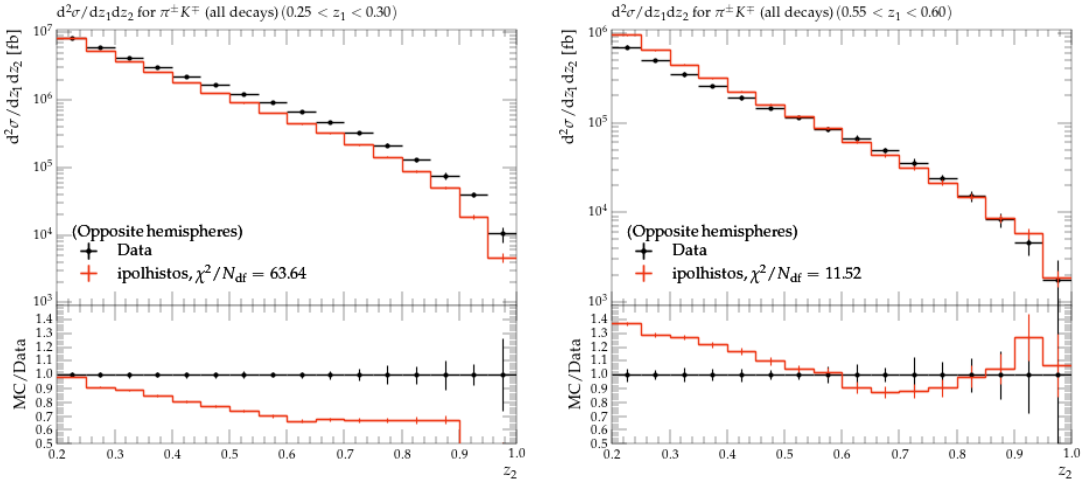

Figure 37: Left: π^+K^- pair cross sections in opposite hemispheres as a function of the invariant mass z_2 for the fractional energy bin $0.25 < z_1 < 0.3$. Right: The same for the fractional energy bin $0.55 < z_1 < 0.6$. The data is displayed by black points while the best fit result in red.

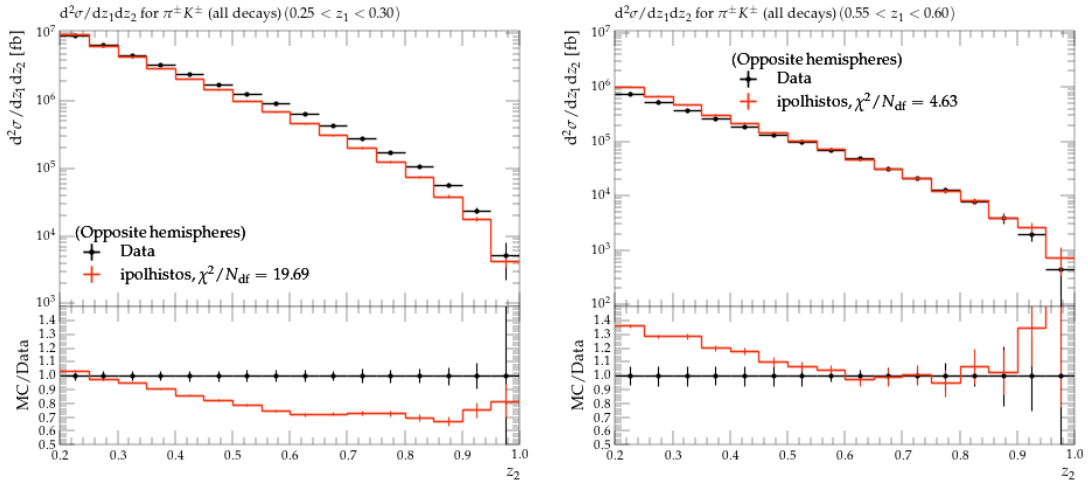

Figure 38: Left: π^+K^+ pair cross sections in opposite hemispheres as a function of the invariant mass z_2 for the fractional energy bin $0.25 < z_1 < 0.3$. Right: The same for the fractional energy bin $0.55 < z_1 < 0.6$. The data is displayed by black points while the best fit result in red.

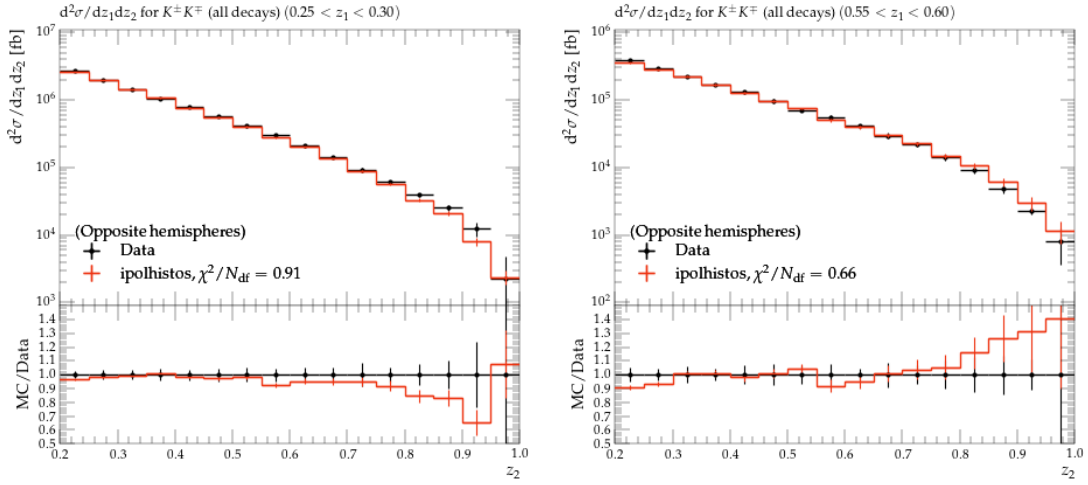

Figure 39: Left: K^+K^- pair cross sections in opposite hemispheres as a function of the invariant mass z_2 for the fractional energy bin $0.25 < z_1 < 0.3$. Right: The same for the fractional energy bin $0.55 < z_1 < 0.6$. The data is displayed by black points while the best fit result in red.

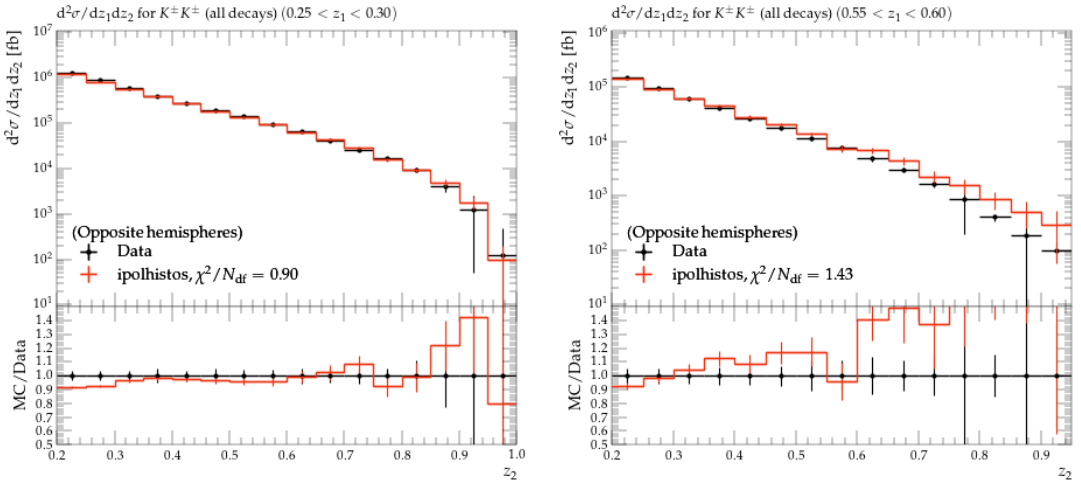

Figure 40: Left: K^+K^+ pair cross sections in opposite hemispheres as a function of the invariant mass z_2 for the fractional energy bin $0.25 < z_1 < 0.3$. Right: The same for the fractional energy bin $0.55 < z_1 < 0.6$. The data is displayed by black points while the best fit result in red.

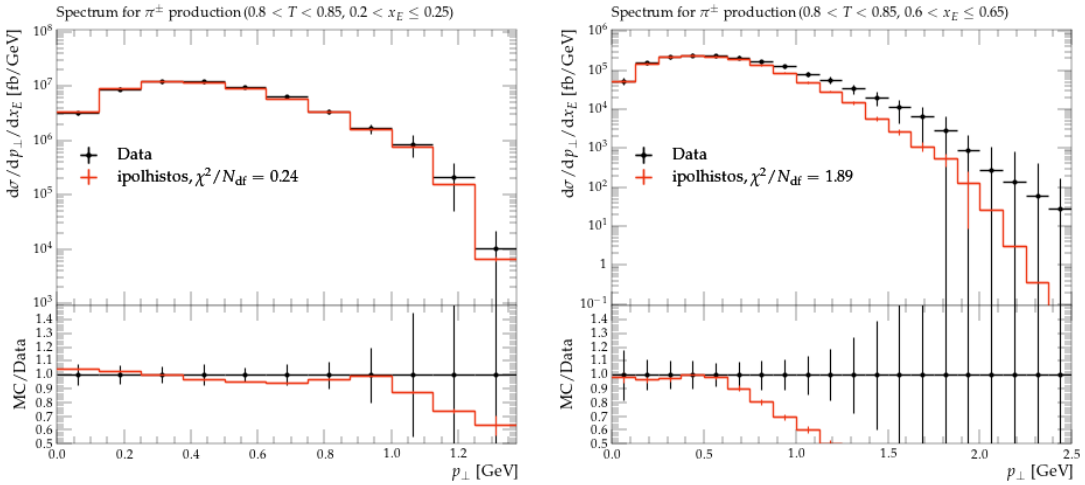

Figure 41: Left: $\pi^\pm$ cross sections as a function of the transverse momentum p_T for the fractional energy bin $0.2 < z_1 < 0.25$ in the thrust bin $0.8 - 0.9$. Right: The same for the fractional energy bin $0.6 < z_1 < 0.65$. The data is displayed by black points while the best fit result in red.

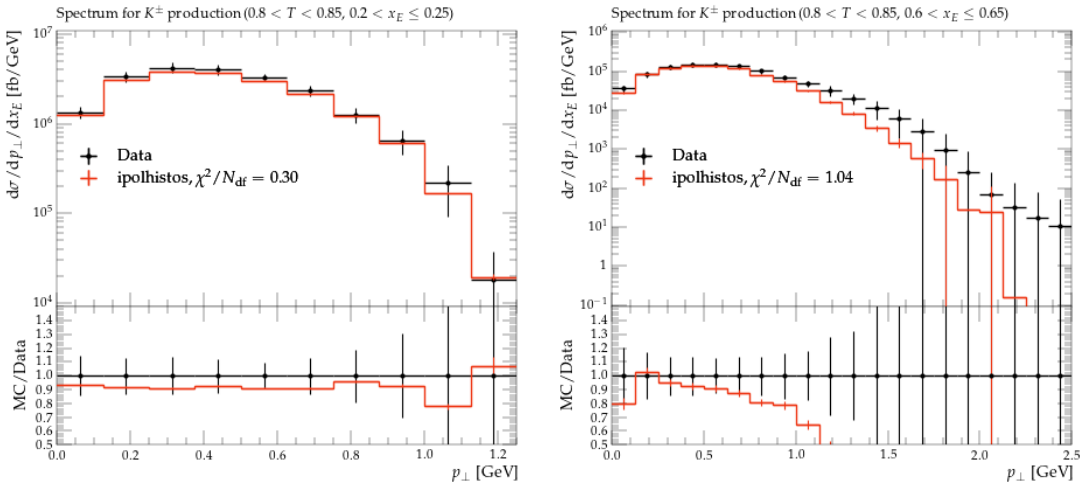

Figure 42: Left: $K^{\pm}$ cross sections as a function of the transverse momentum p_T for the fractional energy bin $0.2 < z_1 < 0.25$ in the thrust bin $0.8 - 0.9$. Right: The same for the fractional energy bin $0.6 < z_1 < 0.65$. The data is displayed by black points while the best fit result in red.

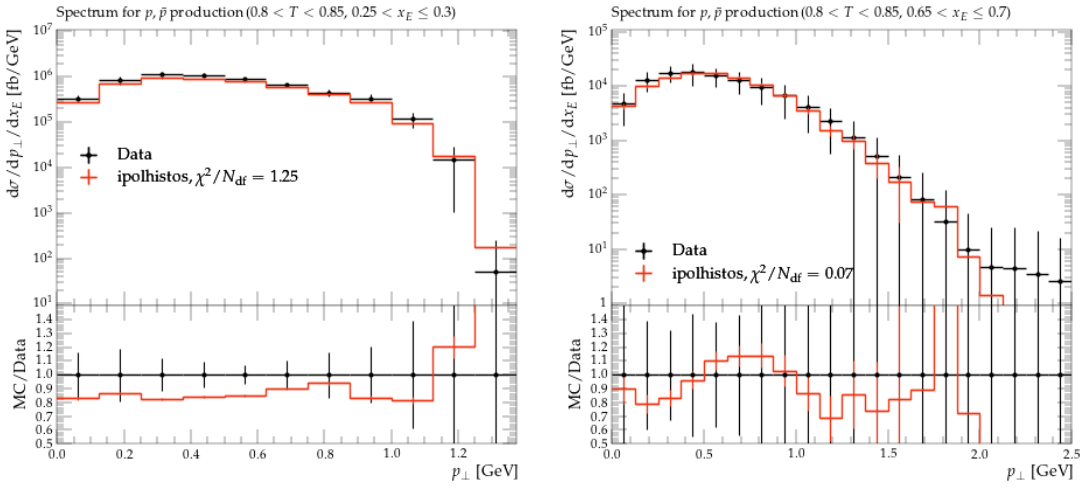

Figure 43: Left: p cross sections as a function of the transverse momentum p_T for the fractional energy bin $0.2 < z_1 < 0.25$ in the thrust bin $0.8 - 0.9$. Right: The same for the fractional energy bin $0.6 < z_1 < 0.65$. The data is displayed by black points while the best fit result in red.

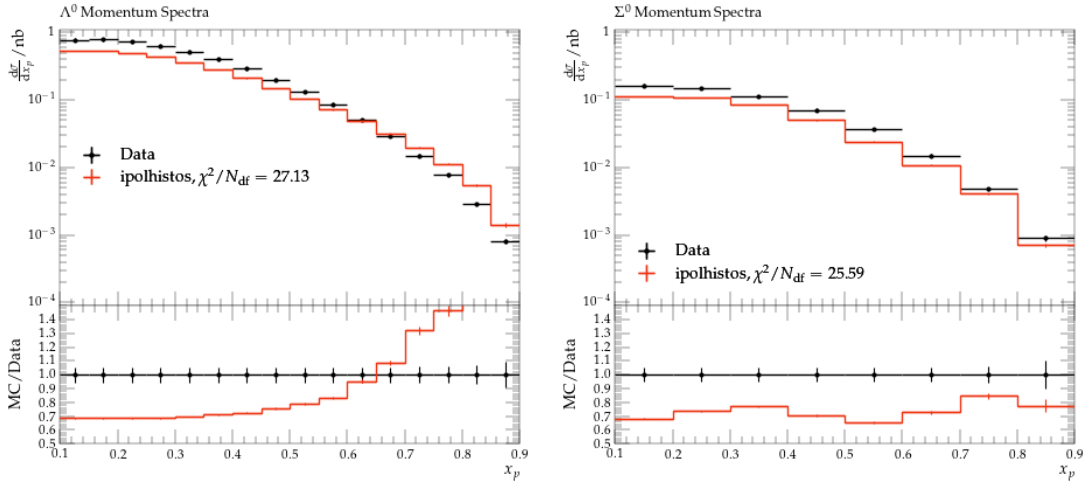

Figure 44: Left: Λ spectrum as a function of x_p. Right Σ^0 spectrum as a function of x_p. The data is displayed by black points while the best fit result in red.

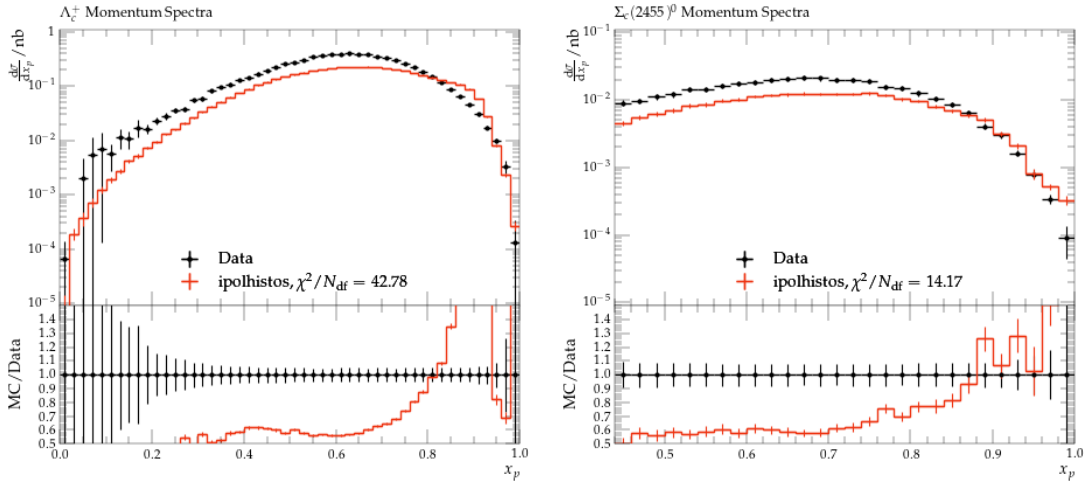

Figure 45: Left: Λ_c^+ spectrum as a function of x_p. Right $\Sigma_c^0(2455)$ spectrum as a function of x_p. The data is displayed by black points while the best fit result in red.

7.5 Hyperons and charmed baryons

For hyperons the description is still not as good, even after including the popcorn variables and used the bug-fixed version of PYTHIA. The overall shapes do have improved, however, as can be seen in Figs. 44 and 45 for some hyperons and charmed baryons, respectively. The peak position of the charmed baryons is somewhat similar to the measurements, but the tune predicts a rather abrupt drop-off of the cross sections at very high momentum fractions that is not confirmed in the data, or at least not as sharp.

8 Systematic uncertainties and tests

The best variables and their variations are summarized in Table 2 in comparison to the default values of PYTHIA and currently in use in Belle2. In this table the best values are given in the second column, the lower and upper values represent the lowest and highest variations of the tune iterations to the best value (i.e. the last iteration for that particular variable). The variations are just given as a measure of how much these variables varied during the tuning evaluations and cannot be considered as reliable uncertainties. In turn, the statistical uncertainties from the tuning efforts are tiny and are therefore not tabulated. One can see that the variables that have been retired after several iterations were quite stable. The corresponding results are also highlighted in Fig. 46 in comparison to the other values.

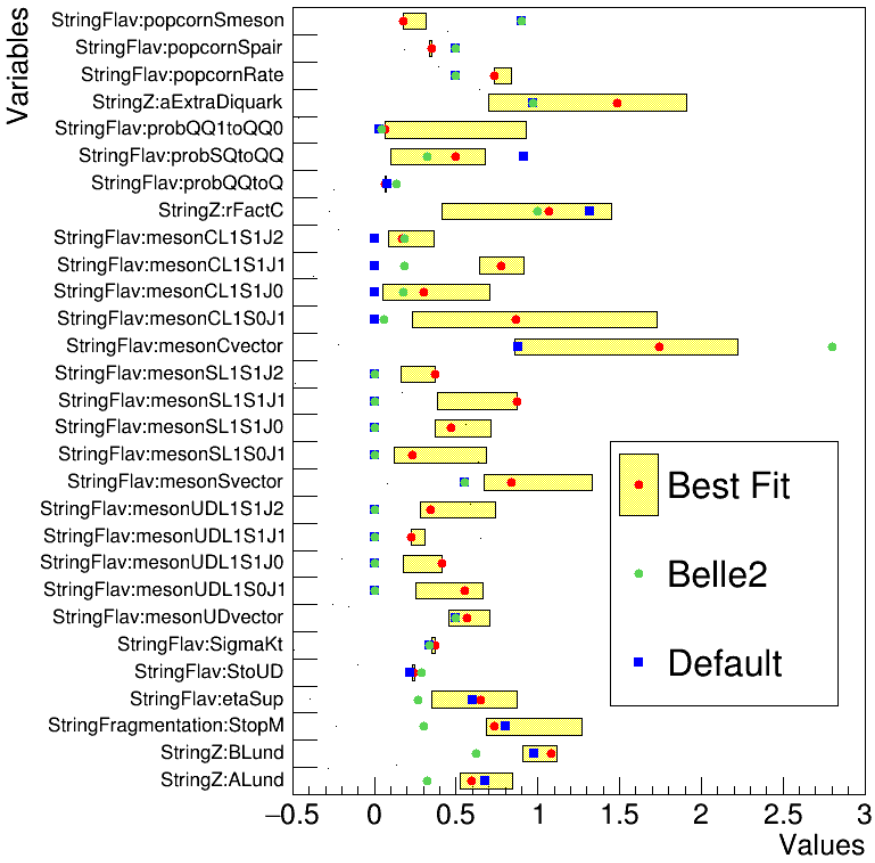

Figure 46: Best tune results (Red points), including their estimated uncertainties as discussed in the text (yellow bars) in comparison to the currently used (Darkgreen) and PYTHIA default (Blue boxes) values for each variable. Due to the significantly larger ranges, the results from mixing angles are not shown.,

The individual sets of variables and their variations are also visualized in the following figures as a function of their iterations. The Main Lund string fragmentation variables can be found in Fig. 47. One sees again that the strangeness suppression and the transverse momentum generation are indeed not changing much over the iterations.

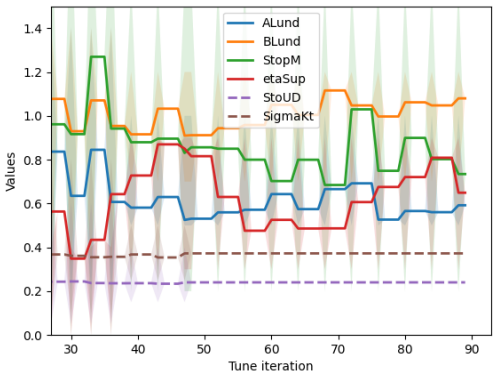

Figure 47: Main Lund variables, the allowed ranges are shown in shaded regions and the best values as a function of the various tuning iterations

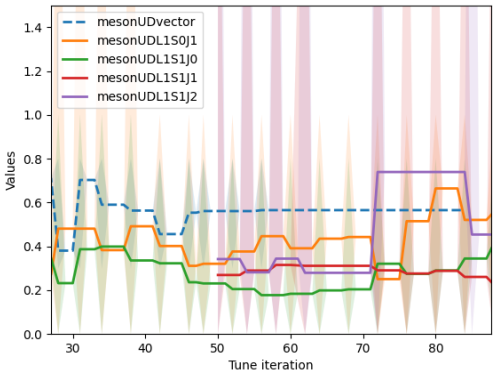

Figure 48: Light quark related vector meson and higher spin variables as a function of the various tuning iterations, the allowed ranges are shown in shaded regions and the best values as the center line. Dashed lines represent variables that have been fixed after they became stable.

The light quark vector meson and higher spin variables can be seen in Fig. 48. Especially the higher spin variables are not particularly well determined and thus fluctuate from iteration to iteration, but the vector meson fraction is fairly stable which is why it was fixed eventually.

The corresponding strange and charm variables are displayed in Figs. 49 and 50, respectively. In these, one can see that the two vector mesons fractions are again the most stable variables and that the charm vector meson fraction is significantly larger than that of strange quarks which again is slightly larger than that for light quarks. The higher spin values typically vary much as well.

The baryon related fragmentation variables are displayed in Fig. 51. Apart from the main diquark fragmentation and the extra Lund factor for diquarks, the values are fluctuating significantly between iterations. After the inclusion of the popcorn values, the vector diquark fraction also appears to stabilize.

The vector and pseudoscalar mixing angles are displayed in Fig. 52. Especially the pseudoscalar mixing value is fluctuating significantly while the vector angle is

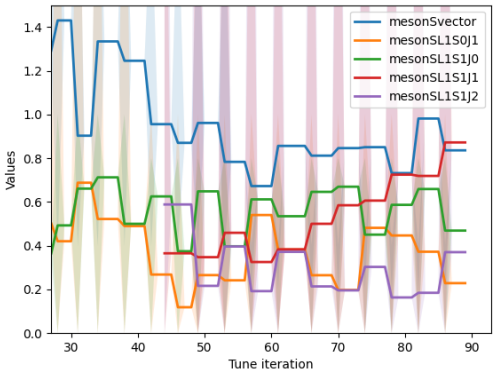

Figure 49: Strange quark related vector meson and higher spin variables as a function of the various tuning iterations, the allowed ranges are shown in shaded regions and the best values as the center line. Dashed lines represent variables that have been fixed after they became stable.

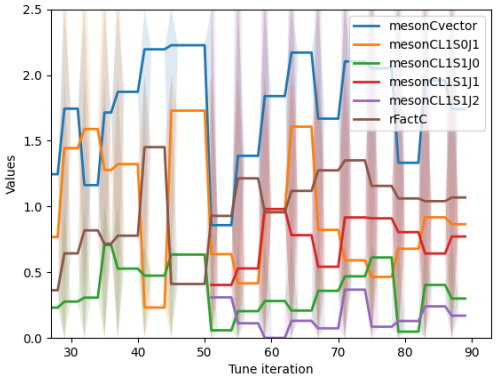

Figure 50: Charm quark related vector meson and higher spin variables as a function of the various tuning iterations, the allowed ranges are shown in shaded regions and the best values as the center line. Dashed lines represent variables that have been fixed after they became stable.

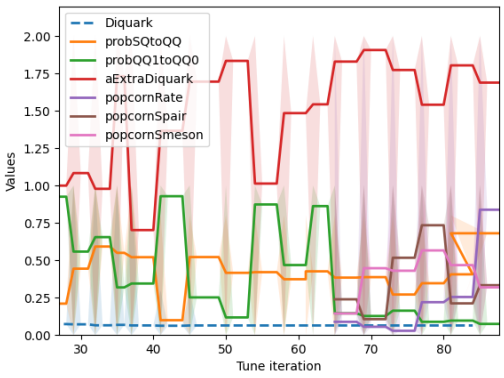

Figure 51: Baryon related variables as a function of the various tuning iterations, the allowed ranges are shown in shaded regions and the best values as the center line. Dashed lines represent variables that have been fixed after they became stable.

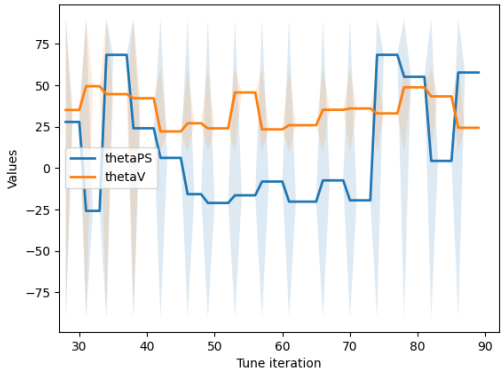

Figure 52: Mixing related variables as a function of the various tuning iterations, the allowed ranges are shown in shaded regions and the best values as the center line. Dashed lines represent variables that have been fixed after they became stable.

slightly more stable.

Last, the evolution of the goodness of fit as a function of the tune iterations is displayed in Fig. 53. One can generally see that the reduced χ^2 did decrease for the most part with the occasional fluctuations. After including the higher spin states and fixing some variables not too much improvement can be seen. Another reduction can be seen when including the popcorn variables at around tune iteration 65, but again after an initial drop the values flatten out. The last improvement can be seen from using the correct treatment of the extra a parameter that was fixed by the PYTHIA maintainers from iteration 77. Since then, the χ^2 does not improve anymore over two further iterations for each set of variables. This suggests that within the space of variables, no significant further improvements can be achieved and likely these are the best settings one can get.

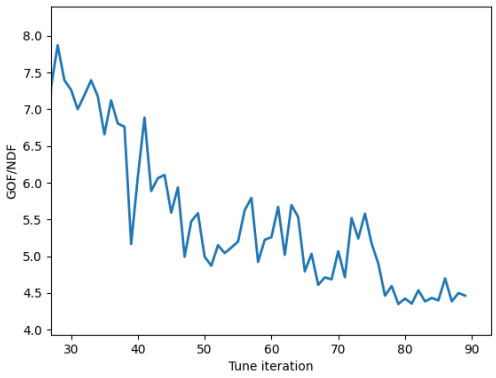

Figure 53: Evolution of the goodness of fit normalized by the number of degrees of freedom as a function of the various tuning iterations.

8.1 Comparison to older settings

It is also instructive to learn how the different settings after tuning compare to the settings used as default or previously at Belle2. Those are displayed for various measurements in the figures 54 to 61. Due to some empty bins in the latest measurements which Rivet cannot handle well, the individual χ^2/NDF for these measurements are given as "nan". It is visible that while individual spectra for very abundant particles such as light mesons are often reasonably well-described by the older settings, especially di-hadron mass or momentum spectra and heavier particles can be much better described after tuning.

Summing up all other χ^2/NDF results gives average values of 15.3 for the Pythia default settings, 14.4 for the previously used Belle2 settings and 6.3 for the latest best settings. Note that these numbers are different from the actual fit numbers since here the average over all individual spectra is taken, rather than summing all points as is done in the fit. Those and the corresponding figures make it abundantly clear, that the tuning effort successfully improved the description of the included measurements.

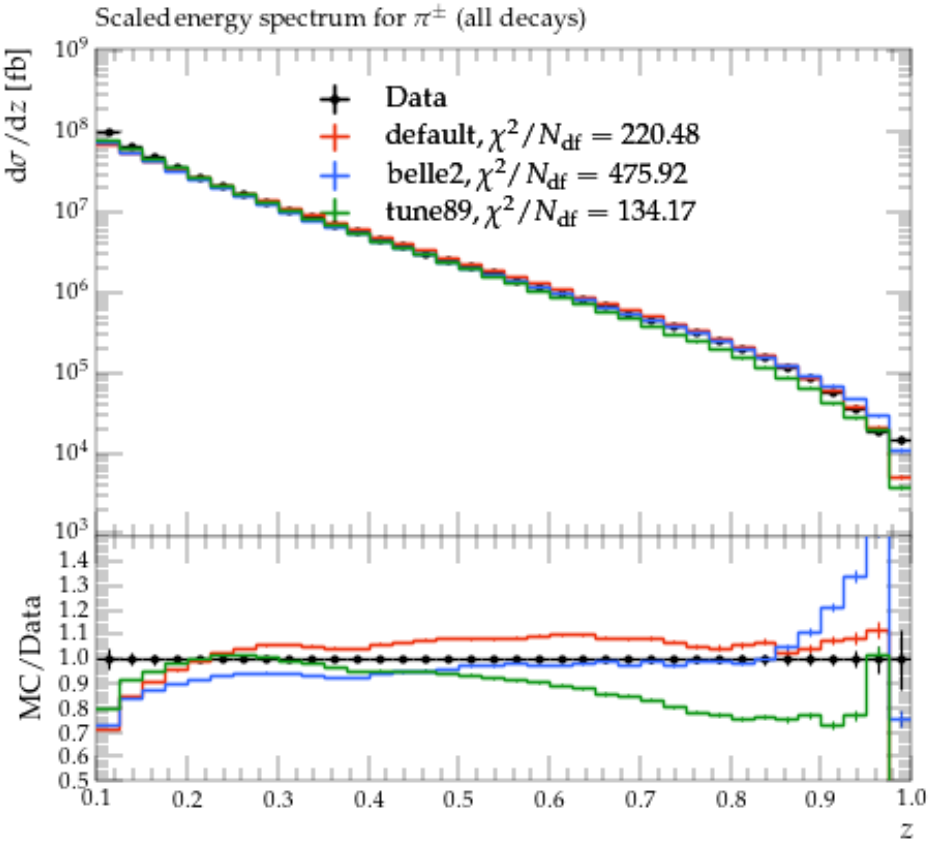

Figure 54: Pion cross sections as a function of the fractional energy z. The data is displayed by black points while the PYTHIA default is displayed in red, the current Belle2 setting in blue, and the best tune in green.

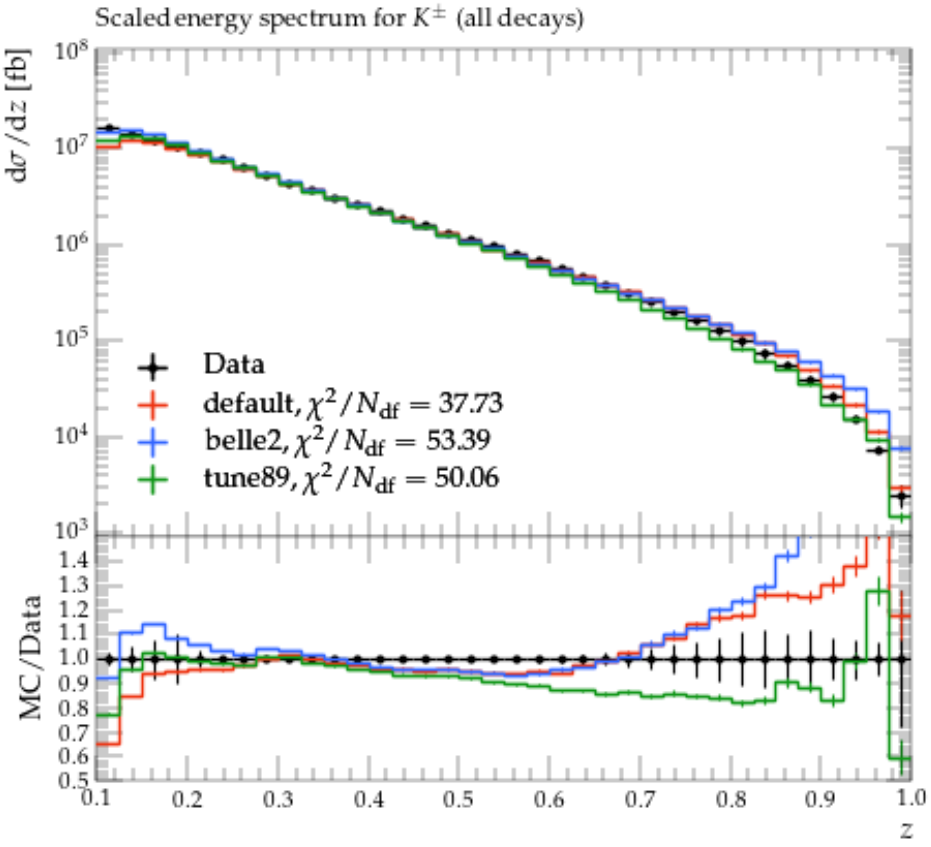

Figure 55: Kaon cross sections as a function of the fractional energy z. The data is displayed by black points while the PYTHIA default is displayed in red, the current Belle2 setting in blue, and the best tune in green.

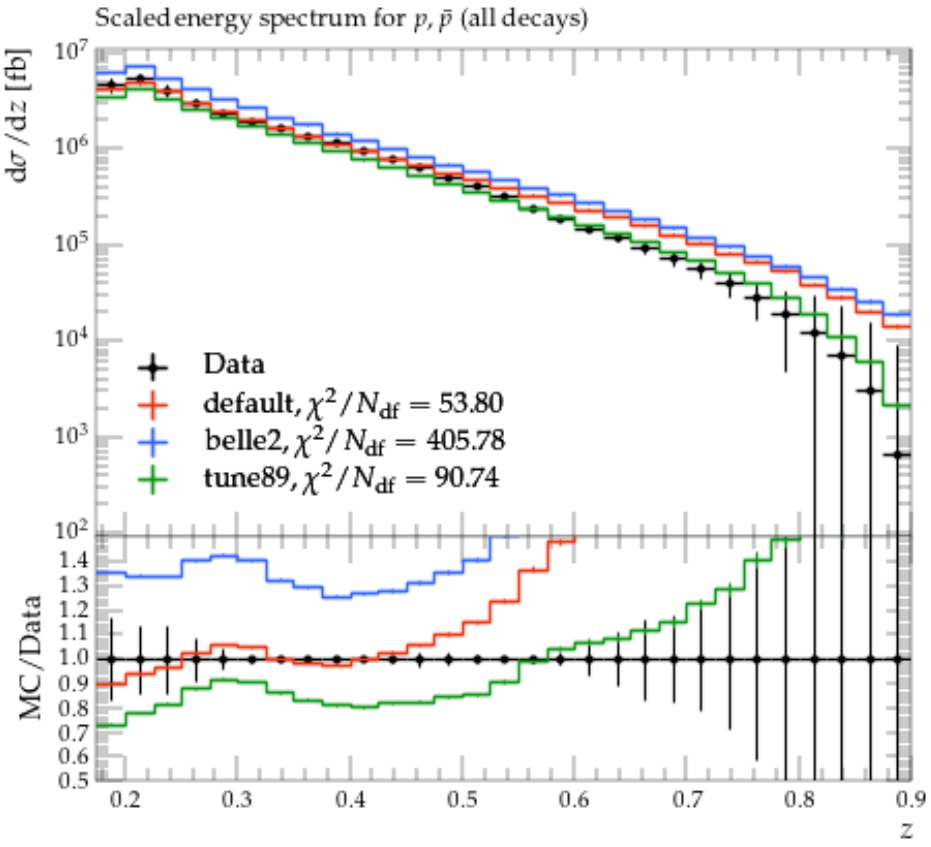

Figure 56: Proton cross sections as a function of the fractional energy z. The data is displayed by black points while the PYTHIA default is displayed in red, the current Belle2 setting in blue, and the best tune in green.

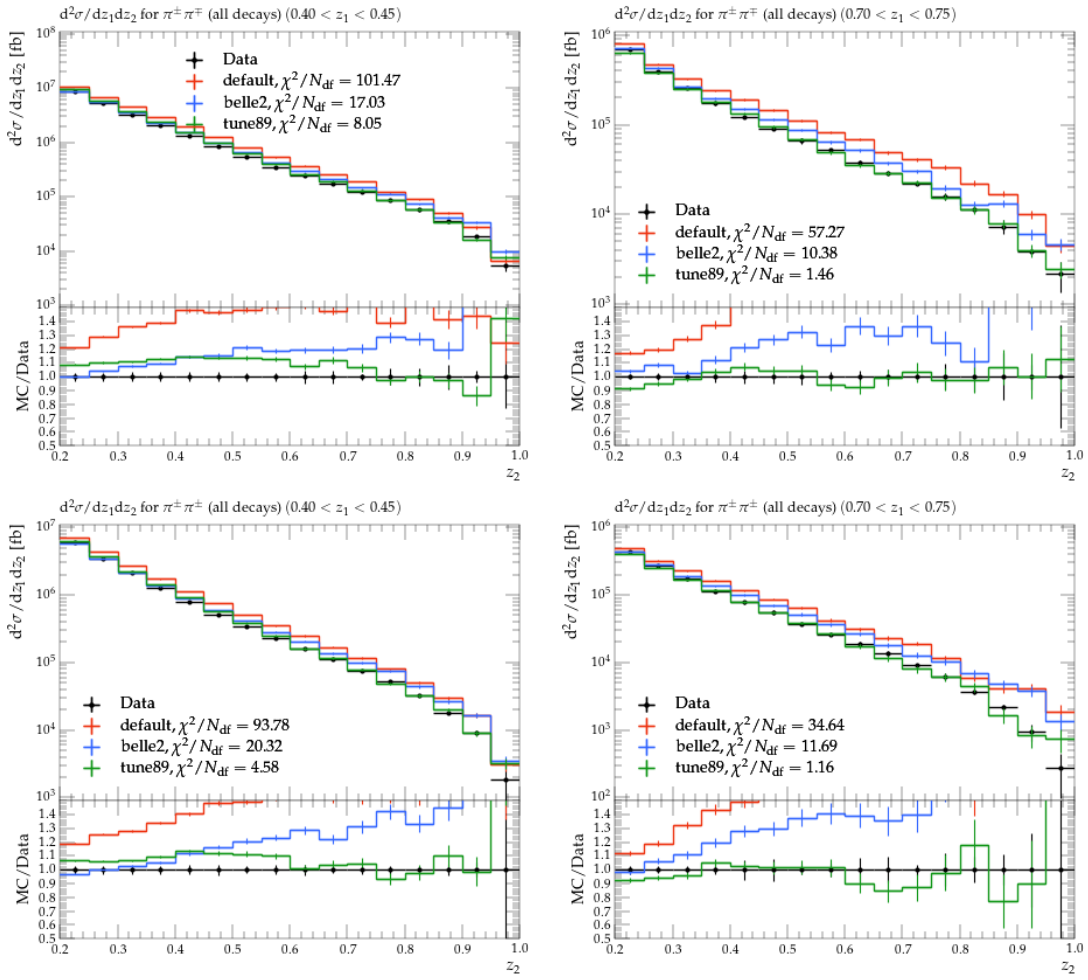

Figure 57: Top: $\pi^+\pi^-$ spectra as a function of z_2 for two bins of z_1. Bottom: $\pi^\pm\pi^\pm$ spectra for the same z bins. The data is displayed by black points while the PYTHIA default is displayed in red, the current Belle2 setting in blue, and the best tune in green.

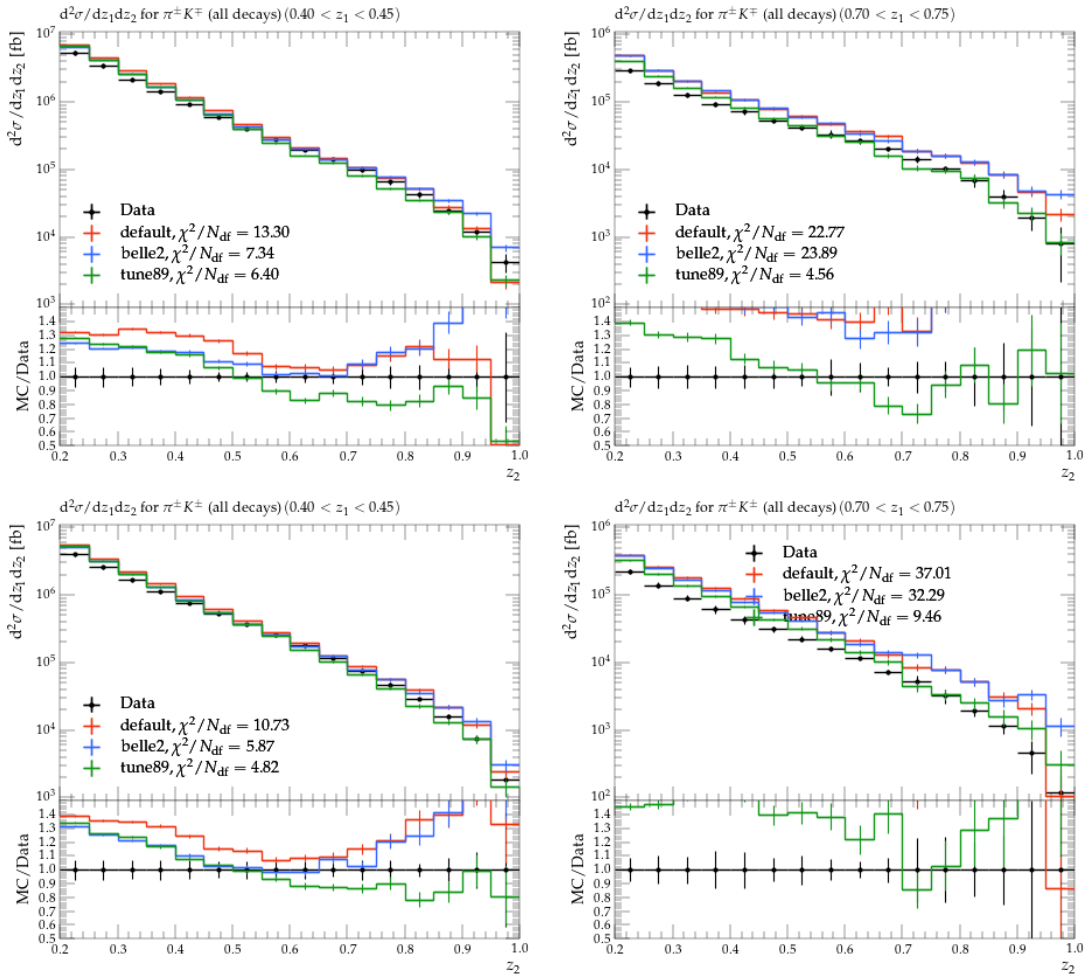

Figure 58: Top: π^+K^- spectra as a function of z_2 for two bins of z_1. Bottom: $\pi^\pm K^\pm$ spectra for the same z bins. The data is displayed by black points while the PYTHIA default is displayed in red, the current Belle2 setting in blue, and the best tune in green.

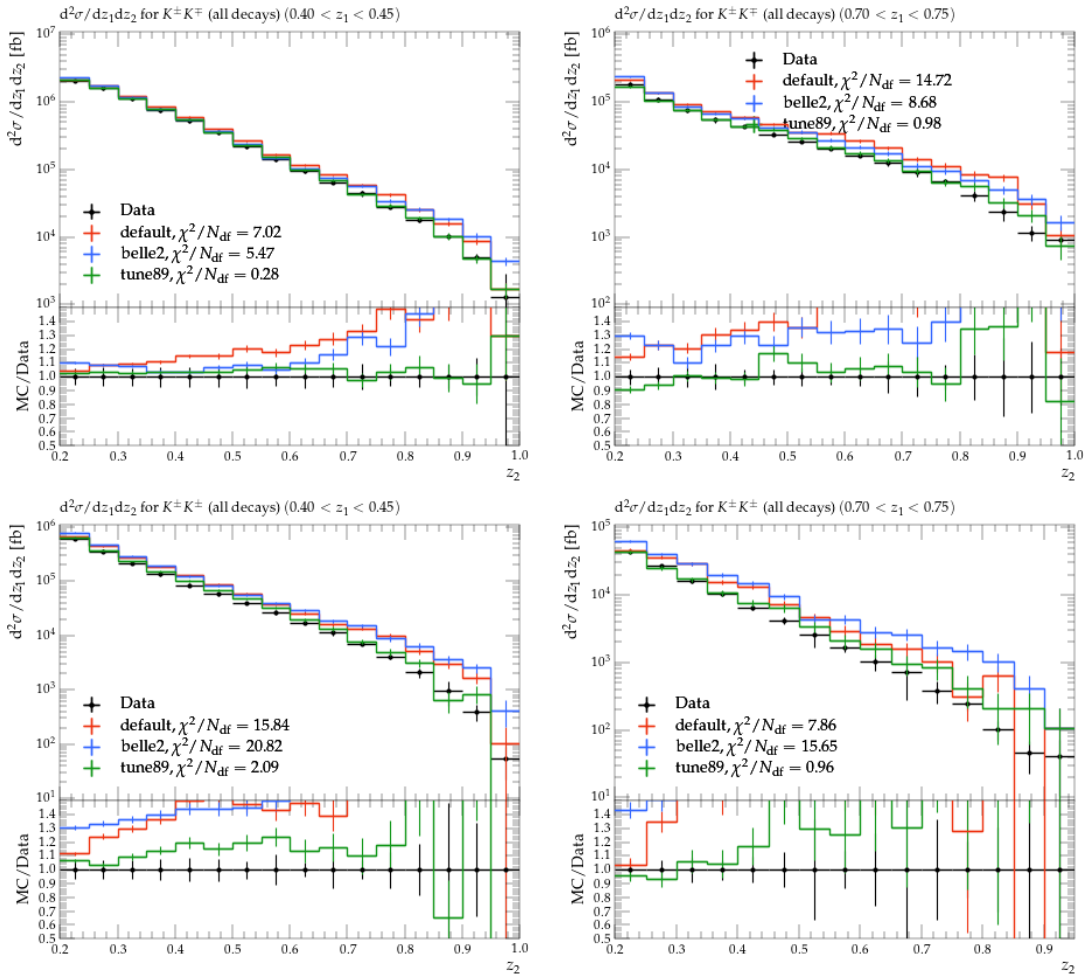

Figure 59: Top: K^+K^- spectra as a function of z_2 for two bins of z_1. Bottom: $K^\pm K^\pm$ spectra for the same z bins. The data is displayed by black points while the PYTHIA default is displayed in red, the current Belle2 setting in blue, and the best tune in green.

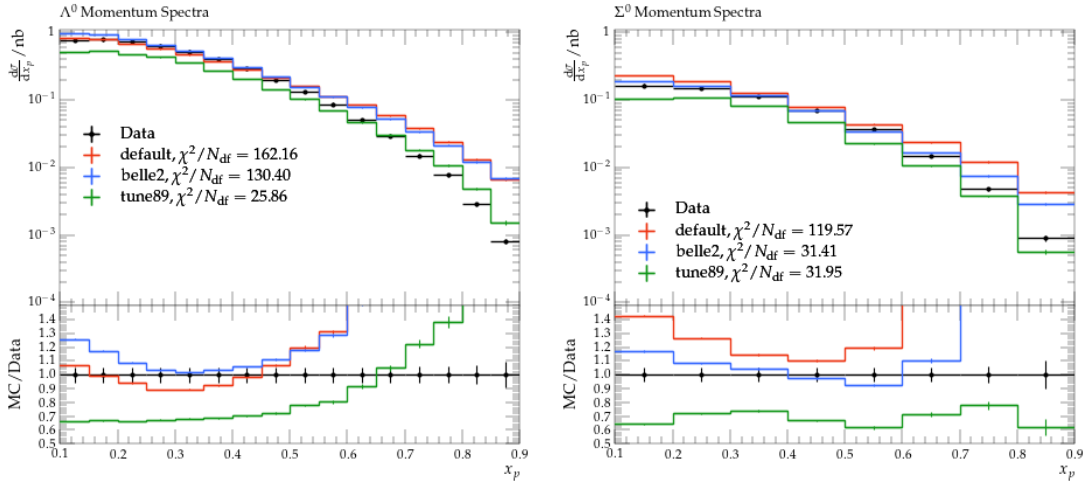

Figure 60: Left: Λ spectrum as a function of x_p. Right Σ^0 spectrum as a function of x_p. The data is displayed by black points while the PYTHIA default is displayed in red, the current Belle2 setting in blue, and the best tune in green.

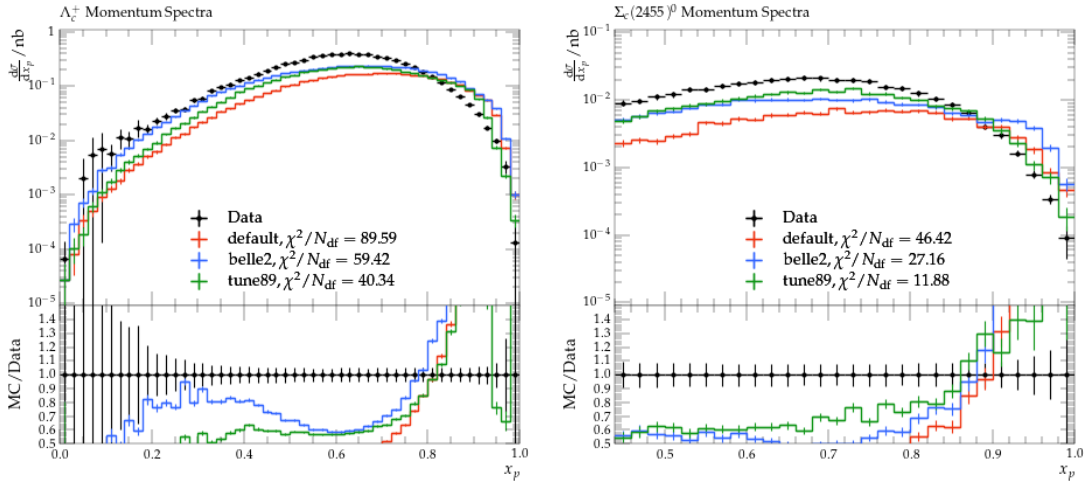

Figure 61: Left: Λ_c^+ spectrum as a function of x_p. Right $\Sigma_c^0(2455)$ spectrum as a function of x_p. The data is displayed by black points while the PYTHIA default is displayed in red, the current Belle2 setting in blue, and the best tune in green.

Table 2: Best tune variables and the variation of the best values during the various tune iterations as well as the PYTHIA default values and the current Belle2 values (release 8/9). Note, that Belle2 has also set the following values etaPrimeSub=0.12, MultIncrease=4.5, and MultIncreaseWeak=2.0 that were not studied here due to lack of sensitivity.

Variable	Best results	default	Belle2
StringZ:ALund	0.592 -0.067 +0.253	0.680	0.32
StringZ:BLund	1.080 -0.170 +0.036	0.980	0.62
StringFragmentation:StopM	0.734 -0.050 +0.535	0.800	0.3
StringFlav:etaSup	0.649 -0.301 +0.221	0.600	0.27
StringFlav:StoUD	0.240 -0.006 +0.004	0.217	0.286
StringFlav:SigmaKt	0.372 -0.019 +0.000	0.335	0.335
StringFlav:mesonUDvector	0.565 -0.109 +0.138	0.500	0.500
StringFlav:mesonUDL1S0J1	0.556 -0.306 +0.108	0	0
StringFlav:mesonUDL1S1J0	0.411 -0.234 +0.000	0	0
StringFlav:mesonUDL1S1J1	0.226 -0.000 +0.086	0	0
StringFlav:mesonUDL1S1J2	0.341 -0.061 +0.399	0	0
StringFlav:mesonSvector	0.836 -0.163 +0.498	0.550	0.550
StringFlav:mesonSL1S0J1	0.229 -0.110 +0.459	0	0
StringFlav:mesonSL1S1J0	0.469 -0.094 +0.243	0	0
StringFlav:mesonSL1S1J1	0.872 -0.489 +0.000	0	0
StringFlav:mesonSL1S1J2	0.370 -0.207 +0.001	0	0
StringFlav:mesonCvector	1.740 -0.882 +0.486	0.880	2.8
StringFlav:mesonCL1S0J1	0.865 -0.634 +0.864	0	0.06
StringFlav:mesonCL1S1J0	0.300 -0.252 +0.408	0	0.1775
StringFlav:mesonCL1S1J1	0.772 -0.129 +0.145	0	0.1868
StringFlav:mesonCL1S1J2	0.170 -0.084 +0.198	0	0.1836
StringZ:rFactC	1.069 -0.658 +0.383	1.32	1.0
StringFlav:probQQtoQ	0.064 -0.002 +0.008	0.081	0.133
StringFlav:probSQtoQQ	0.497 -0.398 +0.184	0.915	0.323
StringFlav:probQQ1toQQ0	0.065 -0.000 +0.864	0.0275	0.0468
StringZ:aExtraDiquark	1.487 -0.785 +0.420	0.970	0.970
StringFlav:popcornRate	0.734 -0.000 +0.104	0.500	0.500
StringFlav:popcornSpair	0.350 -0.016 +0.000	0.500	0.500
StringFlav:popcornSmeson	0.180 -0.000 +0.139	0.900	0.900
StringFlav:thetaPS	57.719 -78.753 +10.675	-15.	-15.
StringFlav:thetaV	24.353 -0.952 +24.444	26.	26.

9 Results

The best results of the tuning exercise are already tabulated in table 1 together with the default values used in PYTHIA8.3 and BelleII. The overall confidence in the best results is high as indicated by the data-tune comparisons in the previous chapters. There are however different levels of how confident the best variables are depending on the overall sensitivities. Based on those, the main Lund parameters are probably very well determined by the tuning as the sensitivities are very high. The vector meson related variables are also fairly well determined thanks to the latest Belle paper [3] which explicitly looked at the fragmentation of vector mesons. The higher spin related variables are somewhat less determined due to the fact that no explicit measurements of these particles are available. There is some indirect sensitivity via the invariant mass distributions where the higher mass ranges get populated from such particle decays. Last, the baryon related variables seem to be also well-determined, but it is obvious by the differences from the tune to the data that the description of baryon fragmentation in the Lund model seems to be still lacking. It will be still better to use the optimized values, but there need to be also significant improvements on the model description itself to really obtain a very reliable description of baryonic final states. As a next step for the BelleII continuum simulation development, it will be important to see whether the optimized settings also directly translate into significant improvements within the overall BelleII simulation framework that uses EvtGen for decays rather than the standalone PYTHIA used in these studies.

References

[1] Bo Andersson, G. Gustafson, G. Ingelman, and T. Sjostrand. Parton Fragmentation and String Dynamics. *Phys. Rept.*, 97:31–145, 1983. doi:10.1016/0370-1573(83)90080-7.

[2] Bo Andersson. *The Lund Model*, volume 7. Cambridge University Press, 1998. doi:10.1017/9781009401296.

[3] R. Seidl et al. Production cross sections of light and charmed mesons in e+e- annihilation near 10.58 GeV. *Phys. Rev. D*, 111(5):052003, 2025. arXiv:2411.12216, doi:10.1103/PhysRevD.111.052003.

[4] Andy Buckley, Hendrik Hoeth, Heiko Lacker, Holger Schulz, and Jan Eike von Seggern. Systematic event generator tuning for the LHC. *Eur. Phys. J. C*, 65:331–357, 2010. arXiv:0907.2973, doi:10.1140/epjc/s10052-009-1196-7.

[5] M. Niiyama et al. Production cross sections of hyperons and charmed baryons from e^+e^- annihilation near $\sqrt{s} = 10.52$˜GeV. *Phys. Rev. D*, 97(7):072005, 2018. arXiv:1706.06791, doi:10.1103/PhysRevD.97.072005.

[6] R. Seidl et al. Invariant-mass and fractional-energy dependence of inclusive production of di-hadrons in e^+e^- annihilation at $\sqrt{s} = 10.58$ GeV. *Phys. Rev. D*, 96(3):032005, 2017. arXiv:1706.08348, doi:10.1103/PhysRevD.96.032005.

[7] R. Seidl et al. Transverse momentum dependent production cross sections of charged pions, kaons and protons produced in inclusive e^+e^- annihilation at $\sqrt{s} = 10.58$ GeV. *Phys. Rev. D*, 99(11):112006, 2019. arXiv:1902.01552, doi:10.1103/PhysRevD.99.112006.

[8] R. Seidl et al. Update of inclusive cross sections of single and pairs of identified light charged hadrons. *Phys. Rev. D*, 101(9):092004, 2020. arXiv:2001.10194, doi:10.1103/PhysRevD.101.092004.

A Pythia StringZ:aExtraDiquark bugfix related changes

As indicated in communication by the PYTHIA team, a bug was found in their porting of the String fragmentation routines from fortran-based sc pythia6 to PYTHIA8 which persisted until version 8.3.14. This bug was related to the handling of the variable StringZ:aExtraDiquark. This behavior was fixed in later versions, but since most tuning efforts using older versions obtained best parameters that included this bug, a switch was introduced to still use the old, incorrect treatment or the corrected one by: StringZ:useOldAExtra = on/off. To test the actual behavior on the Belle2 tuning efforts, the best tune iteration at that time (tune71) was compared for the old, previously used PYTHIA version 8.3.13, and the latest version 8.3.16 either having the old or new treatment explicitly switched on or off. As expected, these changes had no visible effect on any of the meson related measurements used in the tune optimization. When using the old treatment, also no sizable changes were observed for the various baryon measurements, but the behavior between old and new treatment was significantly different. As intended for this variable, the high-z or x_p shapes became softer with the new treatment which resulted in a generally better description of the proton cross sections. Also the behavior of hyperon and charmed baryon cross sections visibly improved while the overall magnitudes are still not well described. The corresponding comparisons are shown in Figs. 62 and 63 for protons, several hyperons and charmed baryons. In these comparisons, it is also visible that the default behavior (i.e. without explicitly setting the StringZ:useOldAExtra = on/off variable) corresponds to the old setting. Because of these changes, and the improvements that go with them, the remainder of the tuning effort was performed using the PYTHIA version 8.3.16 and using the new treatment via StringZ:useOldAExtra = off.

Initially, it was not clear, that the old treatment is still used per default, which resulted in the first tuning efforts after this switch to still use it. Only from tune76 forward the new, correct treatment was explicitly implemented via StringZ:useOldAExtra = off.

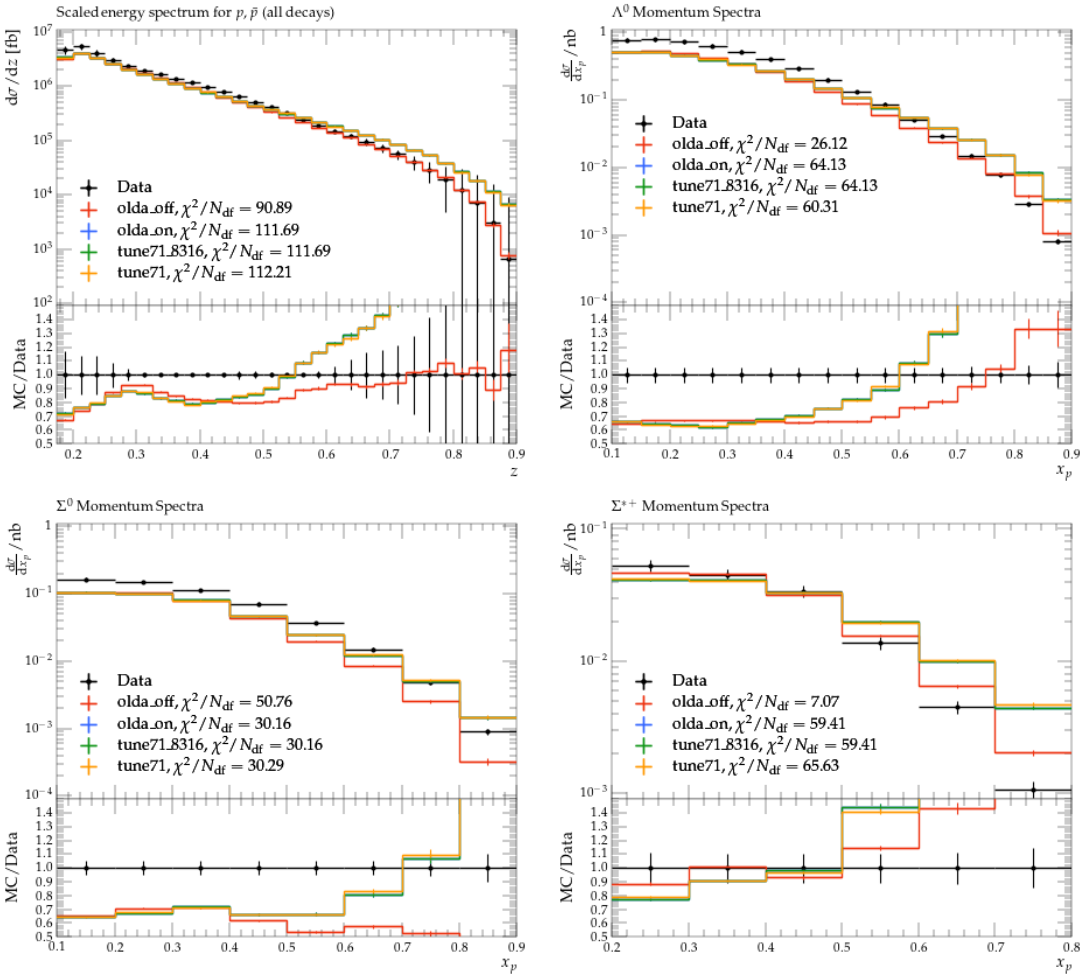

Figure 62: Comparison of the distributions for protons (top left), Λ (top right), Σ^0 (bottom left) and Σ^{*+} as a function of energy or momentum fraction. The black points correspond to the measurements while the yellow points correspond to the best values after tune 71 using PYTHIA8.3.13, the green points correspond to the same tune but using PYTHIA8.3.16, the blue points use the same but explicitly setting StringZ:useOldAExtra to "on", and the red points correspond to the same, but switching it to "off".

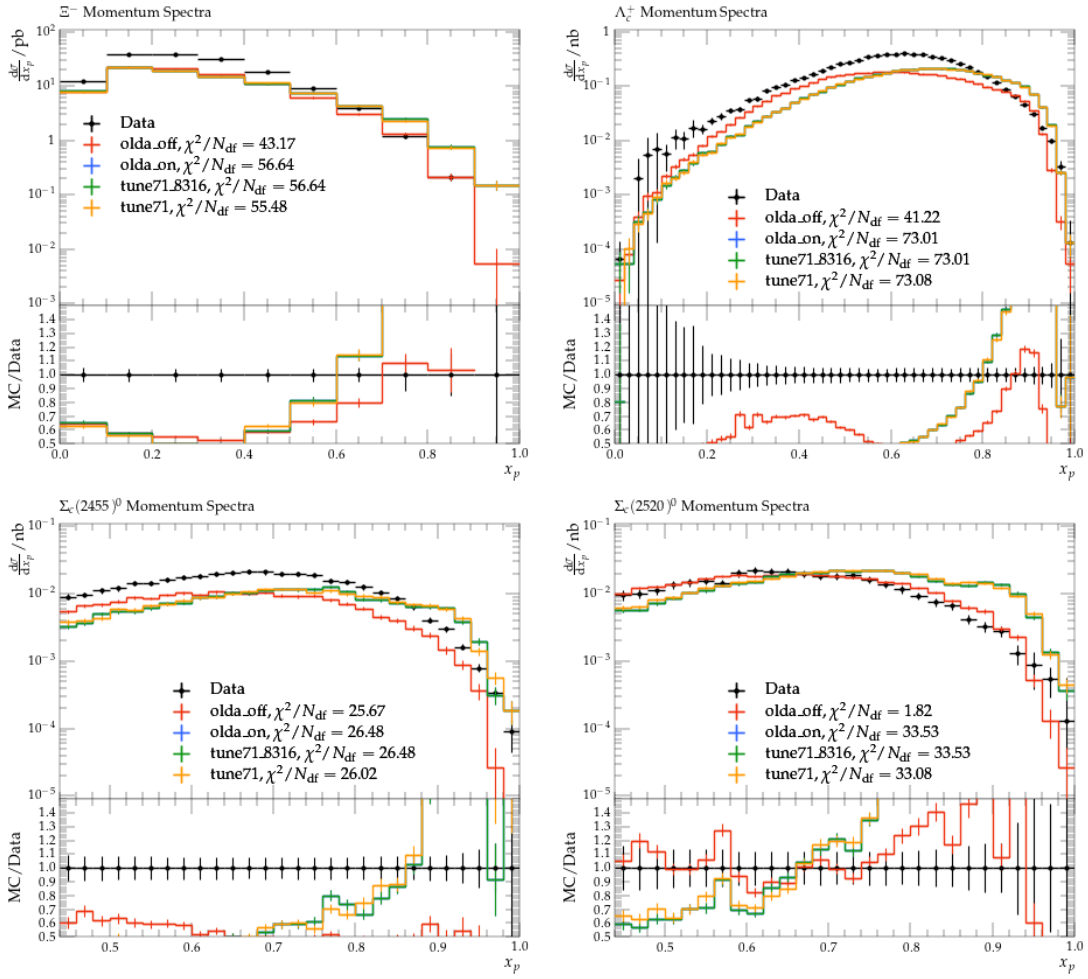

Figure 63: Comparison of the distributions for Ξ^-(top left), Λ_c (top right), $\Sigma_c^0(2455)$ (bottom left) and $\Sigma_c^0(2520)$ as a function of momentum fraction. The black points correspond to the measurements while the yellow points correspond to the best values after tune 71 using PYTHIA8.3.13, the green points correspond to the same tune but using PYTHIA8.3.16, the blue points use the same but explicitly setting StringZ:useOldAExtra to "on", and the red points correspond to the same, but switching it to "off".